AD-A179 941 THEORY OF BELOW-BAND-GAP PHOTOLUMINESCENCE IN A GALLIUM 1/1
ARSENIDE DOPING SUPERLATTICE(U) HARRY DIAMOND LABS
ADELPHI MD J D BRUNO DEC 86 HDL-TR-2100

UNCLASSIFIED F/G 20/12 NL

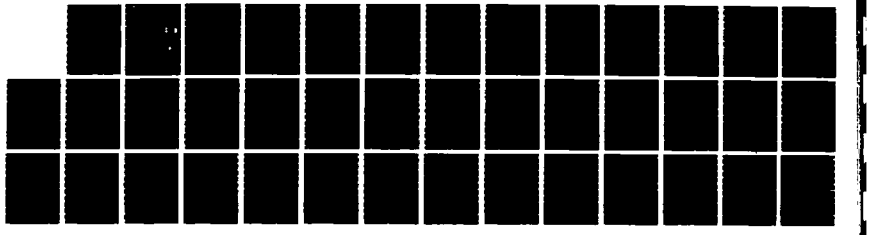

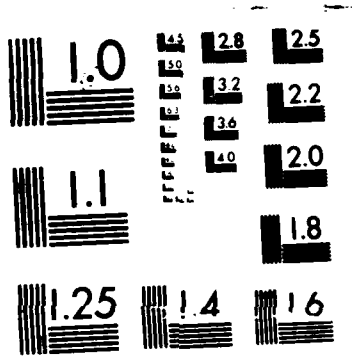

HDL-TR-2100
December 1986

# Theory of Below-Band-Gap Photoluminescence in a Gallium Arsenide Doping Superlattice

John D. Bruno





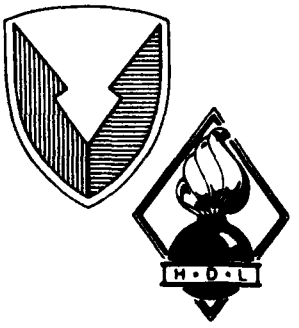


U.S. Army Laboratory Command
**Harry Diamond Laboratories**
Adelphi, MD 20783-1197

The findings in this report are not to be construed as an official Department of the Army position unless so designated by other authorized documents.

Citation of manufacturers' or trade names does not constitute an official indorsement or approval of the use thereof.

Destroy this report when it is no longer needed. Do not return it to the originator.

UNCLASSIFIED AD-A179 941

SECURITY CLASSIFICATION OF THIS PAGE

# REPORT DOCUMENTATION PAGE

| | |
|---|---|
| 1a. REPORT SECURITY CLASSIFICATION<br>UNCLASSIFIED | 1b. RESTRICTIVE MARKINGS |
| 2a. SECURITY CLASSIFICATION AUTHORITY | 3. DISTRIBUTION/AVAILABILITY OF REPORT<br>Approved for public release; distribution unlimited. |
| 2b. DECLASSIFICATION/DOWNGRADING SCHEDULE | |
| 4. PERFORMING ORGANIZATION REPORT NUMBER(S)<br>HDL-TR-2100 | 5. MONITORING ORGANIZATION REPORT NUMBER(S) |
| 6a. NAME OF PERFORMING ORGANIZATION<br>Harry Diamond Laboratories<br>6b. OFFICE SYMBOL (*If applicable*)<br>SLCHD-RT-RA | 7a. NAME OF MONITORING ORGANIZATION |
| 6c. ADDRESS (*City, State, and ZIP Code*)<br>2800 Powder Mill Road<br>Adelphi, MD 20783-1197 | 7b. ADDRESS (*City, State, and ZIP Code*) |
| 8a. NAME OF FUNDING/SPONSORING ORGANIZATION<br>U.S. Army Laboratory Command<br>8b. OFFICE SYMBOL (*If applicable*)<br>AMSLC | 9. PROCUREMENT INSTRUMENT IDENTIFICATION NUMBER |
| 8c. ADDRESS (*City, State, and ZIP Code*)<br>2800 Powder Mill Road<br>Adelphi, MD 20783-1145 | 10. SOURCE OF FUNDING NUMBERS<br>PROGRAM ELEMENT NO. 61101A; PROJECT NO. 1L1611-01A91A; TASK NO.; WORK UNIT ACCESSION NO. |

11. TITLE (*Include Security Classification*)
Theory of Below-Band-Gap Photoluminescence in a Gallium Arsenide Doping Superlattice

12. PERSONAL AUTHOR(S) John D. Bruno

| 13a. TYPE OF REPORT | 13b. TIME COVERED | 14. DATE OF REPORT (*Year, Month, Day*) | 15. PAGE COUNT |
|---|---|---|---|
| Progress | FROM May 86 TO Oct 86 | December 1986 | 42 |

16. SUPPLEMENTARY NOTATION
HDL project: AE9655, AMS Code: P611101.91A

| 17. COSATI CODES | | | 18. SUBJECT TERMS (*Continue on reverse if necessary and identify by block number*) |
|---|---|---|---|
| FIELD | GROUP | SUB-GROUP | |
| 20 | 12 | | Doping, superlattice, photoluminescence, gallium arsenides |
| | | | |

19. ABSTRACT (*Continue on reverse if necessary and identify by block number*)

This report presents a simplified calculation of the photoluminescence spectrum of a gallium arsenide doping superlattice. The electronic states in the conduction band of the superlattice are taken to be harmonic oscillator-like in the doping direction and free particle-like in the transverse directions. Localized acceptor states above the valence band are represented by spherically symmetric hydrogenic functions. Analytic expressions for the electric dipole matrix element between these states are obtained and are employed in the numerical evaluation of the spectrum for different electron-hole distribution functions.

| 20. DISTRIBUTION/AVAILABILITY OF ABSTRACT | 21. ABSTRACT SECURITY CLASSIFICATION | |
|---|---|---|
| ☐ UNCLASSIFIED/UNLIMITED ☒ SAME AS RPT. ☐ DTIC USERS | UNCLASSIFIED | |
| 22a. NAME OF RESPONSIBLE INDIVIDUAL<br>John D. Bruno | 22b. TELEPHONE (*Include Area Code*)<br>(202) 394-2042 | 22c. OFFICE SYMBOL<br>SLCHD-RT-RA |

DD FORM 1473, 84 MAR 83 APR edition may be used until exhausted. All other editions are obsolete.

SECURITY CLASSIFICATION OF THIS PAGE
UNCLASSIFIED

CONTENTS



APPENDICES



FIGURES

FIGURES (cont'd)

## 1. INTRODUCTION

This report contains a simplified calculation of the absorption and photoluminescence spectrum of modulation-doped gallium arsenide for energies below this material's direct band gap. The calculation was motivated by the results of optical experiments [1]* on these systems which, in some cases, revealed a two peak structure in the photoluminescence spectrum whose origin was unclear. The work described below, representing a first attempt at clarifying this situation, is divided into three sections. Section 2 is an overview of the problem beginning with background material and ending with a description of the electronic states used in the calculation. In section 3, the absorption spectrum, the photoluminescence spectrum, and the relationship between them are derived. Finally, section 4 contains a discussion of the theoretical predictions along with critical comments on various simplifications made in the analysis.

## 2. OVERVIEW

The systems from which photoluminescence spectra were obtained consist of approximately 1-μm-thick wafers of gallium arsenide which were grown by molecular beam epitaxy. During growth these samples were selectively doped with donor (Si) and acceptor (Be) impurities at densities in the neighborhood of $10^{18}$ $cm^{-3}$. A typical doping profile appears in figure 1, where a positive ordinate refers to donor (n) doping and a negative one refers to acceptor (p) doping. The abscissa denotes position in the sample measured along a cubic axis (GaAs is a cubic crystal with the zinc blende structure). The periodic nature of the doping profile has led some to refer to these systems as superlattices because of the additional periodic potential† imposed on electrons by the ionized donor and acceptor atoms.

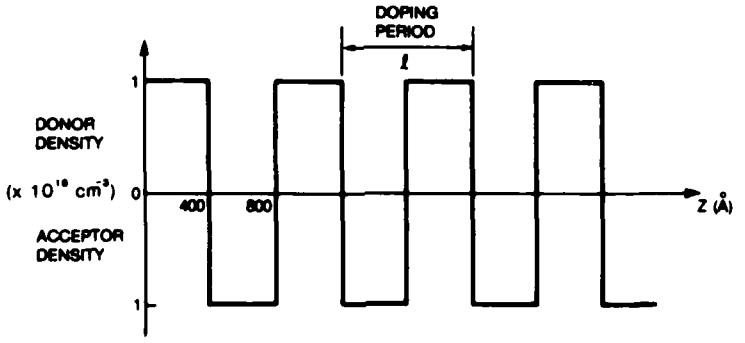


Figure 1. Doping profile along (1,0,0) direction of gallium arsenide crystal.

*References appear at end of text.

†Strictly speaking, the potential is not periodic. Since the impurity atoms are thought to occupy atomic sites in a random manner (at least at these doping densities), the added potential can only be viewed as periodic in the growth direction if one is willing to average over the random distribution of impurities in the transverse directions. This point will be addressed later.

In order to understand the optical properties of this system, one must have a clear picture of the electronic states, and for this, a brief qualitative description of the effects of doping in a single crystal of GaAs is appropriate. Consider first the case of a single donor. Such an impurity differs from the atom it substitutes. In particular, when neutral, it has one extra electron occupying a localized orbital. This electron can be weakly bound to the impurity: its energy might be only 6 meV below the bottom of the conduction band. In such a circumstance, the effective mass theory [2] tells us that all characteristics of the localized state are determined by the nature of the low-energy conduction-band states. For instance, the "Bohr radius" of the impurity wave function is given by $a_B = \hbar^2\kappa/m_c e^2 \approx 100$ Å, where $\kappa$ (=12.5) is the static dielectric constant and $m_c$ is the conduction-band effective mass ($m_c = 0.067$ m; m = electronic mass) of gallium arsenide. At a doping level of $10^{18}$ cm$^{-3}$, the impurities are separated by an average distance of about $10^{-6}$ cm (~100 Å), so that the wavefunctions of impurity states on nearby sites have a substantial overlap. This means that electrons are no longer localized to one impurity but are able to move about throughout the crystal, much like normal conduction-band electrons. This mobility enables electrons to more effectively screen the impurity/electron interaction, weakening its effect. The density of states (DOS) in such a heavily doped system, along with the DOS in the undoped case, is given schematically in figure 2(a). The heavy doping changes the behavior of $\rho(\varepsilon)$ near the band bottom $\varepsilon_c(0)$: in the undoped case $\rho(\varepsilon)$ behaves as $[\varepsilon - \varepsilon_c(0)]^{1/2}$, while in the doped case $\rho(\varepsilon)$ gets a Lorentzian-like contribution to the intrinsic behavior, decreasing the effective band minimum by a small amount (a few milli-electron volts) and adding to the overall DOS above the minimum. As is evident from figure 2(b), the situation is altogether different at these doping densities for acceptor impurities. Unlike donors, acceptors are neutral when their localized state (which lies just above the valence band edge) is unoccupied. Theory predicts the acceptor state in GaAs to have a Bohr radius of about 18 Å ($m_v \cong 0.35\ m_0$), leading to very little overlap between acceptors separated by 100 Å. The states would retain their localized nature and would contribute a relatively sharp peak to the DOS function at an energy above the valence band edge equal to their "binding energy."

Having discussed these simpler cases, we are now in a position to consider a p-n junction and then a superlattice. Figure 3 shows the energy bands versus position along a (1,0,0) direction in GaAs which is p-doped to the left and n-doped to the right of z = 0. The horizontal dash-dot line represents the Fermi energy of the system whereas the heavy dashed line represents the acceptor impurity levels. The manner in which the charges redistribute themselves is responsible for the appearance of figure 3. When the p- and n-doped systems are joined together at z = 0, the mobile electrons in the extended impurity states (z > 0) move into the p-type region (z < 0) occupying acceptor levels. By doing this, electrons can initially lower their energy by ~1.5 eV (the energy gap $E_g$ in GaAs). As more electrons fill states, the vicinity of the junction changes its character: the n-type region becomes positively charged and the p-type region becomes negatively charged. This charge separation creates an electric field which eventually prohibits further charge flow. The total depletion region (where the bands "bend") in this system is about 650 Å wide. This width leads to electric field strengths of about

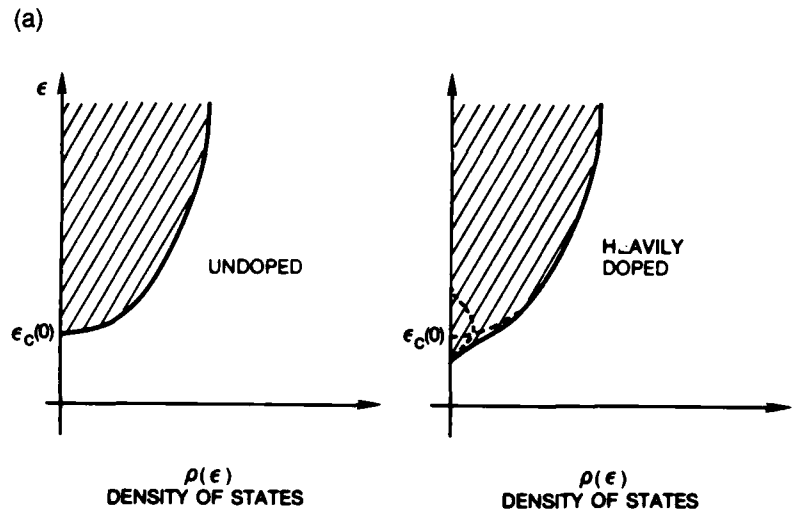


Figure 2. (a) Conduction-band density of states in doped and heavily doped n-type gallium arsenide and (b) valence-band density of states in doped and undoped p-type gallium arsenide.

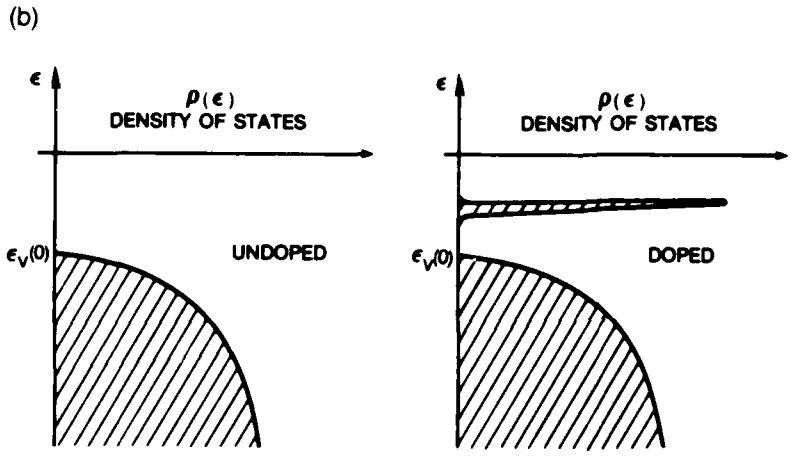


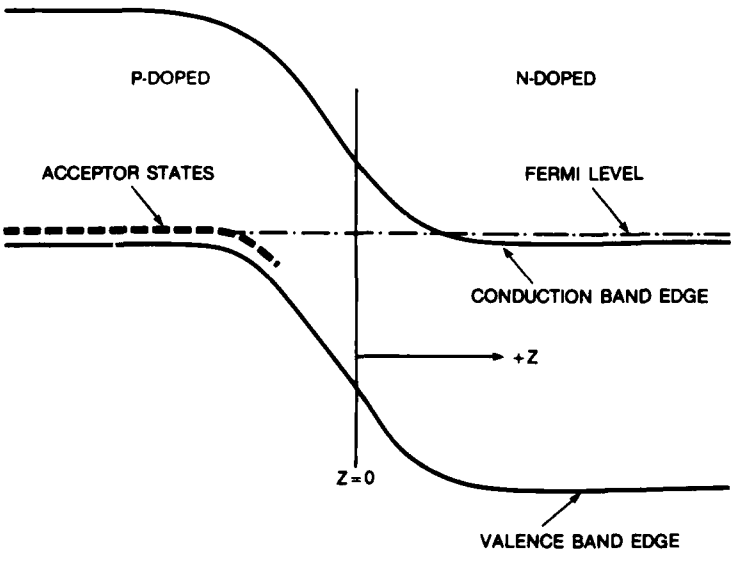


Figure 3. Energy band diagram of gallium arsenide p-n junction at $1 \times 10^{18}$ $cm^{-3}$ doping density.

1.5 V/650 A ~ $10^5$ V/cm. While these fields are large, they are not large enough to invalidate the semiclassical theory [3] of electron dynamics (which goes into the arguments leading to fig. 3). This theory allows us to assume that the spectrum of single-particle states at a position $z_1$ is the same as that found at $z_2$, with the exception of an overall constant shift in all energies by $e[\phi(z_2) - \phi(z_1)]$ where e is the magnitude of the electronic charge and $\phi$ is the electrostatic potential set up by the ionized impurities. The validity of the semiclassical approach implies, among other things, that the DOS above the conduction-band minimum in figure 3 is like that shown (roughly) in figure 2(a) for all values of z. In particular, a continuum of single-particle states begins at the band bottom even for a z-coordinate within the depletion region.

We are now in a position to consider the nature of the electronic states in a crystal of GaAs which has been doped according to the profile in figure 1. Because the n and p doping densities are equal and because the doping period $\ell$ is significantly less than the normal depletion width (650 A) in a GaAs p-n junction at these doping densities, the lowest energy configuration of this system would correspond to completely ionized donors and acceptors: no region of the superlattice will be charge free. The results of a semiclassical approach to obtaining the electronic structure for this system are displayed in figure 4. The conduction-band bottom (and valence-band top) in this figure is obtained by adding to the unperturbed band structure $\varepsilon^{(0)}(\mathbf{k})$ the potential energy $U(z) = -e\phi(z)$. This potential energy can be obtained by "smoothing out" the localized ions to form alternating layers (of thickness $\ell/2$) of uniform positive and negative charge density.* We then need to solve $\nabla^2\phi(z) = -4\pi\rho(z)$ with $\rho(z) = \pm eN_d$, where the upper (lower) sign refers to n-doped (p-doped) regions and $N_d$ is the donor (and acceptor) density. This calculation is simple, and leads to figure 4, with $U_0$ given by $U_0 = \pi N_d e^2 \ell^2/8\kappa$ (which for the parameters of fig. 1 equals 290 meV).

Unfortunately, the semiclassical approach is easily shown to be inadequate in this case. A calculation of the kinetic energy (KE) required by an electron localized in one of the conduction-band wells of figure 4 gives KE ~ 3 meV. This energy would represent the typical separation between low-lying states inside the well, leading to a DOS far below that predicted by the semiclassical picture where the states are more dense by a factor of at least 500. We are thus forced to employ the effective mass theory in order to obtain the electronic states. This has been done for the conduction-band states by Ruden and Döhler [4]. Their results show that near the bottom of the wells in the conduction band (and the top of the valence-band wells), the electronic states are harmonic oscillator-like in the z-direction and free electron-like in the transverse directions. An electron in one of these states is confined in the z-direction and free in the x-y plane. The effective oscillator frequency is easily obtained via the identification $1/2(m_c\omega_0^2 z^2) = 1/2(4\pi N_d e^2/\kappa)z^2$, giving $\omega_0 = (4\pi N_d e^2/m_c\kappa)^{1/2}$. The valence band

*The approximation of replacing the impurity potential $\phi(\mathbf{r})$ by its average $\phi_{ave}(\mathbf{r})$ is probably a good one because the typical difference between the two, $\langle|\phi_{ave}(\mathbf{r}) - \phi(\mathbf{r})|\rangle$, is less than the kinetic energy gained from one electron in its delocalization (which is proportional to the impurity-impurity overlap).

is more complicated because in GaAs, the valence-band maximum (at $\mathbf{q} = \mathbf{0}$) is four-fold degenerate (including spin). In addition, the effective masses are quite different from the conduction-band mass. These two facts complicate the structure. In the present work this complication is ignored (comments regarding its importance will be made in sect. 4). In figure 5 a schematic of the electronic structure is given along with a DOS profile in the conduction and valence bands (the valence-band profile is included only to emphasize its qualitative difference from the DOS profile of fig. 2(b)). Note in particular the step-like nature of these profiles, which is characteristic of a two-dimensional system (the DOS in a two-dimensional system of free electrons is a constant). The acceptor state energies are represented by a dashed line whose position should not be taken too seriously since our treatment of the valence-band states [5]* has been approximate.

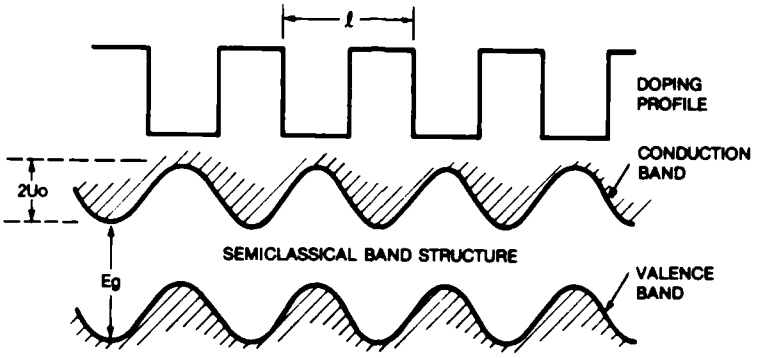


Figure 4. Energy band diagram of system in semi-classical approximation.

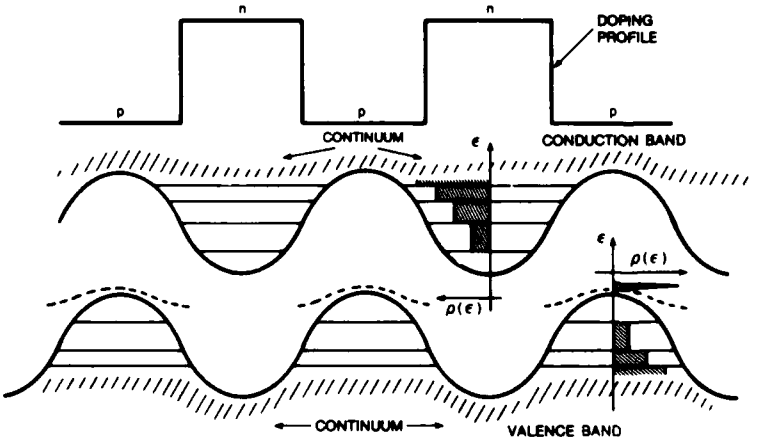


Figure 5. Energy band diagram of system in effective mass approximation including density of states profiles in the conduction- and valence-band wells. For clarity, finite width of minibands has been ignored.

*A preliminary calculation of acceptor binding energies versus position in a superlattice (which ignores valence-band structure) was made by Leavitt and Simpson [5] and supports qualitatively the positional dependence of the binding energies which is displayed in figure 5.

In light of this electronic structure, the novel optical (and electrical) properties of this system are readily understood in a qualitative way. The ground state has all acceptor levels filled with electrons, and the conduction-band states are empty. If one excites electron-hole pairs with an above-direct-band-gap cw laser (e.g., a He-Ne laser), electrons will scatter off phonons on a $10^{-12}$ s time scale [6], eventually relaxing into the lowest conduction-band states possible. Similarly, holes will relax to the highest acceptor states available. The radiative recombination time for electrons and holes, which in a uniformly doped semiconductor is of order $10^{-9}$ s [6], is dramatically increased because of the reduced overlap between low-energy electron states and acceptor states whose wave functions are separated by up to a superlattice half period (200 Å in this system). As a result of this reduction in recombination rates, a cw laser will initially create electron-hole pairs more rapidly than they can recombine, leading to a filling of electron states in the conduction band and hole states in the acceptor levels. As this filling proceeds, the recombination rate rapidly increases for two reasons. First, higher oscillator states in the well extend further out, giving them greater overlap with acceptor wave functions. Second, and more important, as the steady-state nonequilibrium charge density in the conduction band (and acceptor levels) increases, the effective potential seen by an electron is weakened by the carrier's increased ability to screen the space charge field of the ionized impurities. Any weakening of this potential will dramatically increase conduction-band-state/acceptor-state overlap, resulting in higher radiative recombination rates. When the generation and recombination rates are equal, a steady state will be reached. This steady state will be characterized by an effective potential that differs markedly from the potential seen in the absence of excitation. This means that each pump laser intensity will correspond to a specific steady-state charge density in the conduction band, $n^{(2)}$, and its corresponding effective potential. Figure 6 schematically shows the situation one obtains in this system at two different pump laser intensities ($I_b > I_a$). The higher charge density in b results in a substantially weakened potential and increased effective gap $\tilde{E}_g$.

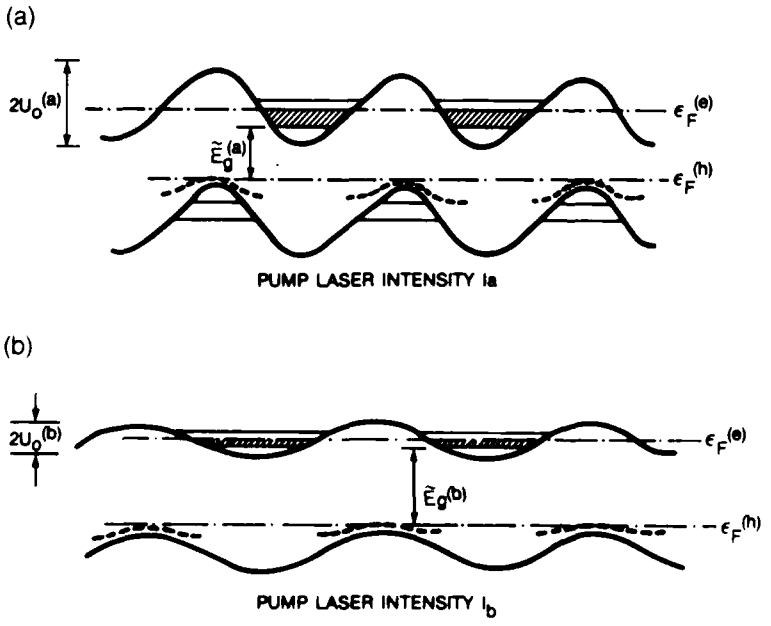


Figure 6. Energy band diagrams representing two steady-state nonequilibrium configurations of superlattice. Pump laser intensity which maintains steady state is higher in (b) than in (a), resulting in a larger effective gap.

In the analysis that follows, we obtain the photoluminescence spectrum $R_{sp}$, where $R_{sp}$ is defined as the energy of recombination radiation falling into the energy interval $d\varepsilon$ at $\varepsilon$ (per unit volume, per unit time). It is assumed that in a quasi-equilibrium steady state there is a sharp quasi-Fermi level in the conduction band below which all electronic states are occupied. We take the valence band to be full and the number of empty acceptor states (unoccupied hole states) equal to the total number of occupied conduction-band states. Near-band-gap recombination radiation is due to electrons making transitions from the occupied conduction-band states into the unoccupied acceptor states. An electron confined in a conduction-band well will have a substantial probability of making a transition into acceptor levels only in neighboring p-type regions. In view of this, we first fix our attention on a given well and a single acceptor level whose center is located a distance $z_0$ from the well minimum.

The states in the well are described in the effective mass theory by wave functions of the form

$$\psi(\mathbf{r}) = F_c(\mathbf{r}) u_{c,0}(\mathbf{r}) \quad . \tag{1}$$

Here $u_{c,0}(\mathbf{r})$ is the Bloch function corresponding to the lowest energy conduction-band state and $F_c(\mathbf{r})$ is a modulating function that satisfies the equation

$$\left[ -\frac{\hbar^2}{2m_c} \nabla^2 + \frac{1}{2} m_c \omega_0^2 z^2 \right] F_c(\mathbf{r}) = \varepsilon F_c(\mathbf{r}) \quad , \tag{2}$$

where $\varepsilon$ is the energy measured with respect to the conduction-band effective potential minimum (at $z = 0$) and $m_c$ is the conduction-band effective mass. Because of the translational invariance of this Hamiltonian in directions normal to the z-axis, $F_c$ can be written

$$F_c(\mathbf{r}) = e^{i\mathbf{k}\cdot\mathbf{r}} \eta(z) \quad , \tag{3}$$

where $\mathbf{k} \equiv (k_x, k_y, 0)$ with $k_i = (2\pi/L) n_i$ ($n_i = 0, \pm 1, \pm 2, \ldots$; $i = x,y$). Unless otherwise stated, $\mathbf{k}$ will always refer to a two-dimensional vector ($k_z \equiv 0$). We take a system composed of $N_\ell$ periods of length $\ell$ such that $\ell N_\ell = L$. The cross-sectional area of each layer is $L^2$, so that the total volume of the system is $\Omega = L^3$. Substituting equation (3) into equation (2) leads to the harmonic oscillator equation for $\eta$

$$\left[ -\frac{\hbar^2}{2m_c} \frac{d^2}{dz^2} + \frac{1}{2} m_c \omega_0^2 z^2 \right] \eta(z) = \left( \varepsilon - \frac{\hbar^2 k^2}{2m_c} \right) \eta(z) \quad , \tag{4}$$

whose solutions [7] can be written

$$\eta_\nu(z) = \sqrt{L}\, 2^{-\nu/2}\, \nu!^{-1/2}\, \pi^{-1/4}\, b^{-1/2}\, e^{-z^2/2b^2} H_\nu(z/b) \quad , \tag{5}$$

where $b = (\hbar/m_c\omega_0)^{1/2}$, $H_\nu(y)$ are Hermite polynomials, and $\nu$ labels the oscillator energy levels. The eigenvalues $\varepsilon$ in equation (4) take the form $\varepsilon_\nu(\mathbf{k}) = \hbar^2k^2/2m_c + \hbar\omega_0(\nu + 1/2)$. We have chosen to normalize the wave function according to the requirement

$$\int_\Omega d\mathbf{r}|\psi(\mathbf{r})|^2 = 1 \quad ,$$

$$N \int_{\Omega_0} d\boldsymbol{\rho}|u_{c,0}(\boldsymbol{\rho})|^2 = 1 \quad ,$$

where N is the number of unit cells in the system and the second integral is over the volume occupied by a unit cell $\Omega_0$.

A particularly simple form has been chosen for the acceptor states: one which ignores entirely the previously mentioned complications in the valence band by treating the highest energy valence-band state as nondegenerate (except for spin). The wave functions are of the form

$$\psi_a(\mathbf{r}) = F_v(\mathbf{r})u_{v,0}(\mathbf{r}) \quad , \tag{6}$$

where $u_{v,0}(\mathbf{r})$ is the highest energy valence-band Bloch function, and $F_v$ is a modulating function* satisfying a hydrogen-like Schroedinger equation. For simplicity, $F_v$ is taken to have the hydrogenic form

$$F_v(\mathbf{r}) = \left(\frac{\Omega}{\pi a^3}\right)^{1/2} e^{-r/a} \quad , \tag{7}$$

where a is the acceptor-state Bohr radius and $\vec{r}$ measures position with respect to the impurity.

## 3. CALCULATION

We begin an analysis of this system's optical properties by determining its absorption coefficient. In this calculation we assume that a monochromatic plane wave is incident on the superlattice which is in its ground state. The Hamiltonian of the system is given by $H = H_0 + H_1$, where $H_0$ gives rise to the harmonic oscillator-like and acceptor states described earlier, and $H_1$, given by $H_1 = (e/mc)\mathbf{A}\cdot\mathbf{P}$, represents the interaction of an electron with an external electromagnetic field. The field, which is assumed to be linearly polarized in the $\hat{\varepsilon}$ direction ($\hat{\varepsilon}\cdot\hat{z} = 0$) and propagating through the sample in the z-direction, can be expressed in the form

$$\mathbf{E} = E_0(\omega)\hat{\varepsilon}\, e^{i(qz-\omega t)} + c.c. \quad , \tag{8}$$

---

*More properly, one would have $\psi_a(\mathbf{r}) = \sum_\mu F_\mu(\mathbf{r})u_{v,0,\mu}(\mathbf{r})$ for the acceptor level, where the sum on $\mu$ is over all degenerate ($q = 0$) valence-band states (and maybe even other nearby bands) and the $F_\mu(\mathbf{r})$ are modulating functions satisfying a set of coupled differential equations. See reference 2.

where $q = (\omega/c)n$ and n is the refractive index of GaAs. This field is derivable from the vector potential

$$\mathbf{A} = A_0(\omega)\hat{\varepsilon}e^{i(qz-\omega t)} + \text{c.c.} \quad , \tag{9}$$

with $\mathbf{E} = -(1/c)\,\partial\mathbf{A}/\partial t$ and $A_0(\omega) = cE_0(\omega)/i\omega$.

For absorption we are interested in the rate at which $H_1$ induces transitions between the acceptor levels and the conduction-band states. Labelling an acceptor state, which is centered at (0, 0, $z_0$), by "a" and conduction-band state by "$\nu,\mathbf{k}$" we obtain, using Fermi's Golden Rule [7], the rate of induced transitions from $|a\rangle$ to $|\nu,\mathbf{k}\rangle$:

$$W_{\nu k,a} = \frac{2\pi}{\hbar}\,|\langle\nu,\mathbf{k}|H_1(\omega)|a\rangle|^2\;\delta\left(\varepsilon_{\nu,\mathbf{k}} - \varepsilon_a(z_0) - \hbar\omega\right) \quad , \tag{10}$$

where $\varepsilon_a(z_0)$ is the energy of the acceptor state (measured with respect to the effective potential minimum of the conduction band). Since we want to determine the rate at which energy is taken out of the radiation field, we should multiply this by $\hbar\omega$ and then sum over all final states $|\nu,\mathbf{k}\rangle$. The delta function will ensure that only states with the proper energy are included in the sum. (Inspection of fig. 7 shows that for a given $\hbar\omega$, a set of pairs $\{\nu,\mathbf{k}_\nu\}$ will conserve energy.) Therefore we can write

$$W = \hbar\omega \sum_{\nu}\sum_{\mathbf{k}} \frac{2\pi}{\hbar}\,|\langle\nu,\mathbf{k}|H_1(\omega)|a\rangle|^2\;\delta\left(\varepsilon_{\nu,\mathbf{k}} - \varepsilon_a(z_0) - \hbar\omega\right) \quad , \tag{11}$$

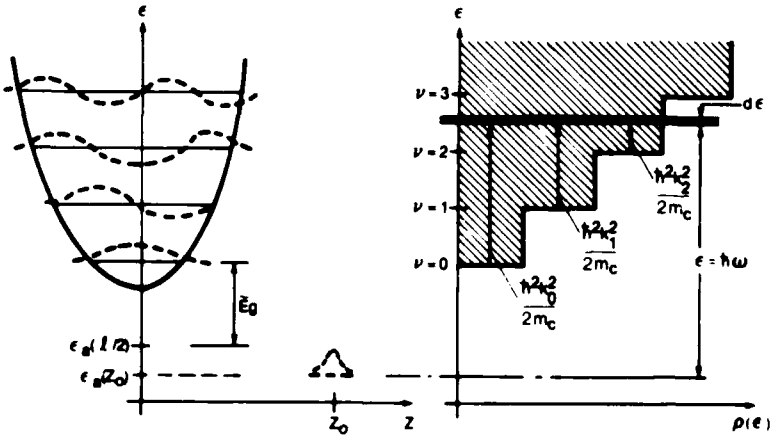


Figure 7. Conduction-band-well effective oscillator and density of states along with a single hydrogenic acceptor wavefunction located a distance $z_0$ from well minimum.

where W is the rate at which energy is absorbed from the radiation field via transitions out of *one* acceptor level. If we use the relation

$$\sum_{\mathbf{k}} 1 = \frac{L^2}{(2\pi)^2} \int 2\pi k \frac{dk}{d\varepsilon_{\nu,k}} d\varepsilon_{\nu,k} = \frac{L^2 m_c}{2\pi\hbar^2} \int d\varepsilon_{\nu,k}$$

and include a factor of 2 for spin, equation (11) becomes

$$W(z_0) = \frac{2L^2 m_c \omega}{\hbar^2} \sum_{\nu} |\langle \nu k_\nu | H_1(\omega) | a \rangle|^2 \theta(k_\nu^2) \quad , \tag{12}$$

where $k_\nu^2 \equiv (2m_c/\hbar^2)\{\hbar\omega - \hbar\omega_0(\nu + 1/2) + \varepsilon_a(z_0)\}$ and $\theta(x) \equiv 1$ for $x > 0$ and 0 for $x < 0$.

In order to determine the effects of all the impurity states, we can refer to figure 8, where we have schematically plotted the acceptor levels versus position along with the neighboring conduction-band wells. The contribution from transitions out of an acceptor to its neighboring two wells will be $W(z_0) + W(\ell - z_0)$. The number of acceptors in the slab with thickness $dz_0$ at $z_0$ is $L^2 dz_0 N_d$. We can then integrate over $z_0$ from $\ell/4$ to $3\ell/4$ and multiply the result by $N_\ell$, the number of periods, to get

$$N_\ell \int_{\ell/4}^{3\ell/4} dz_0 N_d L^2 \left[W(z_0) + W(\ell - z_0)\right] \quad .$$

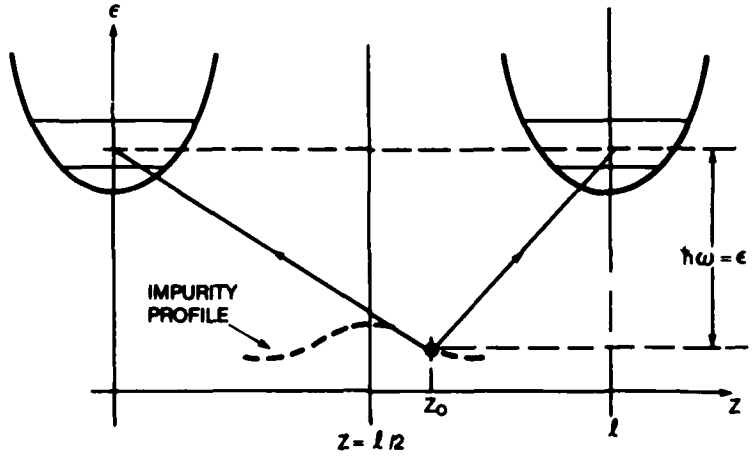


Figure 8. Acceptor energy profile along with neighboring conduction-band wells.

Because of the obvious symmetry about $z = \ell/2$, this becomes

$$2N_d N_\ell L^2 \int_{-\ell/4}^{\ell/4} dx\, W\left(\frac{\ell}{2} + x\right) \quad .$$

Using $N_\ell \ell = L$ and dividing by $L^3$, we obtain the total rate of energy loss per unit volume

$$\frac{W_{total}}{L^3} = \frac{2N_d}{\ell} \int_{-\ell/4}^{\ell/4} dx\, W\left(\frac{\ell}{2} + x\right) \quad . \tag{13}$$

This rate is simply connected to the absorption coefficient $\alpha(\omega)$. Imagine a wave entering a slab of thickness t. On entering, the wave's intensity is $I_0$ $(=(nc/8\pi)\ |E_0|^2)$, while on leaving it is $I_0 e^{-\alpha t}$. So, the net energy into the slab per unit time is $I_0 L^2 - I_0 e^{-\alpha t} L^2 \simeq I_0 \alpha t L^2$. This gives $I_0\alpha$ for the net energy into the slab per unit time, per unit volume. Equating this to the expression above gives

$$\alpha(\omega) = \frac{2N_d}{I_0 \ell} \int_{-\ell/4}^{\ell/4} dx\, W\left(\frac{\ell}{2} + x\right) \quad . \tag{14}$$

To proceed further, we need to evaluate $W(z_0)$ as given in equation (12). Consider first the matrix element $\langle \nu, \mathbf{k}_\nu | H_1(\omega) | a \rangle$. This can be written

$$\langle \nu, \mathbf{k}_\nu | H_1(\omega) | a \rangle = \int_\Omega d\mathbf{r}\, u^*_{c,0}(\mathbf{r}) F^*_c(\mathbf{r}) \left(\frac{e}{mc} \mathbf{A}(\omega)\cdot\mathbf{P}\right) u_{v,0}(\mathbf{r}) F_v\left(\mathbf{r} - z_0\hat{z}\right) \quad . \tag{15}$$

If we now make the replacements

$$\mathbf{r} \to \mathbf{R}_i + \boldsymbol{\rho} \quad , \quad \int_\Omega d\mathbf{r} \to \sum_i \int_{\Omega_0} d\boldsymbol{\rho} \quad ,$$

and, in the spirit of the effective mass theory, ignore changes in the modulating functions on the length scale of a lattice constant, we obtain

$$\begin{aligned} \langle \nu, \mathbf{k}_\nu | H_1(\omega) | a \rangle = \frac{e}{mc} \mathbf{A}(\omega)\cdot \Bigg\{ & \sum_i F^*_c(\mathbf{R}_i) \mathbf{P} F_v\left(\mathbf{R}_i - z_0\hat{z}\right) \int_{\Omega_0} d\boldsymbol{\rho}\, u^*_{c,0}(\boldsymbol{\rho}) u_{v,0}(\boldsymbol{\rho}) \\ & + \sum_i F^*_c(\mathbf{R}_i) F_v\left(\mathbf{R}_i - z_0\hat{z}\right) \int_{\Omega_0} d\boldsymbol{\rho}\, u^*_{c,0}(\boldsymbol{\rho}) \mathbf{P} u_{v,0}(\boldsymbol{\rho}) \Bigg\} \quad . \end{aligned} \tag{16}$$

The first term in braces is zero because in GaAs, the functions $u_{c,0}$ and $u_{v,0}$ have different symmetry* and so are orthogonal. Keeping only the second term and using $A_0(\omega) = cE_0(\omega)/i\omega$ leads to

$$\langle \nu, \mathbf{k}_\nu | H_1(\omega) | a \rangle = \frac{eE_0}{i\omega m} \left(\hat{\varepsilon} \cdot \mathbf{P}_{c,v}(0)\right) \frac{1}{\Omega} \int_\Omega d\mathbf{R}\, F_c^*(\mathbf{R}) F_v\left(\mathbf{R} - z_0 \hat{z}\right) \quad , \tag{17}$$

where we have defined† $\mathbf{P}_{c,v}(0) \equiv N \int_{\Omega_0} d\boldsymbol{\rho}\, u_{c,0}^*(\boldsymbol{\rho}) \mathbf{P} u_{v,0}(\boldsymbol{\rho})$. The integral in equation (17) can be done more easily if we first Fourier transform $F_v$, replacing it with

$$F_v(\mathbf{x}) = \sum_{\mathbf{q}} C(\mathbf{q}) e^{i\mathbf{q}\cdot\mathbf{x}} \quad .$$

The transform $C(\mathbf{q})$ is easily shown to be

$$C(\mathbf{q}) = \left(\frac{64\pi a^3}{\Omega}\right)^{1/2} \frac{1}{(1 + q^2a^2)^2} \quad ,$$

and when used in equation (17) gives

$$\langle \nu, \mathbf{k}_\nu | H_1(\omega) | a \rangle = \frac{eE_0}{i\omega m} \left(\varepsilon \cdot \mathbf{P}_{c,v}(0)\right) \sum_{q_z} C(\mathbf{k}_\nu, q_z) \tilde{\eta}_\nu(-q_z) e^{-iq_z z_0} \quad , \tag{19}$$

where

$$\tilde{\eta}_\nu(q_z) \equiv \frac{1}{L} \int_{-\infty}^{\infty} dz\, \eta_\nu(z) e^{-iq_z z} \quad \text{and} \quad C\left(\mathbf{k}_\nu, q_z\right) \equiv C\left(k_{\nu_x}, k_{\nu_y}, q_z\right) \quad .$$

Consider now the calculation of $\tilde{\eta}_\nu(q_z)$. If we define

$$N_\nu = \sqrt{L}\, 2^{-\nu}\, \nu!^{-1/2}\, \pi^{-1/4}\, b^{-1/2}$$

and use the dimensionless variable $y = z/b$, we can write

$$\tilde{\eta}_\nu(q_z) = \frac{N_\nu b}{L} \int_{-\infty}^{\infty} dy\, e^{-y^2/2} H_\nu(y) e^{-iq_z b y} \quad . \tag{20}$$

---

*s-like and p-like, respectively.

†Because of the normalization convention chosen for the u's, the factor of N is needed to make the result finite.

Although this integral can be done, it is more useful at this point to define $\tilde{\eta}_\nu(q_z)$ in terms of derivatives of the Hermite polynomial generating function. For this we define

$$I_\nu(\alpha) = \int_{-\infty}^{\infty} dy\ e^{-y^2/2}\ e^{-i\alpha y}\ H_\nu(y)$$

and its generating function $F(s,\alpha)$:

$$F(s,\alpha) = \sum_{\nu=0}^{\infty} \frac{I_\nu(\alpha)S^\nu}{\nu!} = \int_{-\infty}^{\infty} dy\ e^{-y^2/2}\ e^{-i\alpha y} \sum_\nu \frac{H_\nu(y)S^\nu}{\nu!} \quad . \tag{21}$$

Since $\sum_\nu \frac{H_\nu(y)c^\nu}{\nu!} = e^{-s^2+2sy}$ [7], we obtain after doing the integral,

$$F(s,\alpha) = \sqrt{2\pi}\ e^{\alpha^2/2-2i\alpha s} \quad . \tag{22}$$

Using this expression along with the generating function allows for a determination of $I_\nu(\alpha)$ with the rule

$$I_\nu(\alpha) = \frac{d^\nu}{ds^\nu} F(s,\alpha)\bigg|_{s=0} \quad . \tag{23}$$

*Combining these results in equation (20) then gives*

$$\tilde{\eta}_\nu(q_z) = \frac{N_\nu b}{L}\sqrt{2\pi}\ e^{-q_z^2b^2/2}\ \frac{d^\nu}{ds^\nu}\left(e^{s^2-2iq_zbs}\right)\bigg|_{s=0} \quad . \tag{24}$$

After $\tilde{\eta}_\nu(-q_z)$ is substituted into equation (19), the matrix element becomes

$$\langle \nu,\mathbf{k}_\nu|H_1(\omega)|a\rangle = \frac{eE_0}{i\omega m}\left(\hat{\epsilon}\cdot\mathbf{P}_{c,v}(0)\right)\frac{C(\mathbf{0})}{\sqrt{2\pi}}\ N_\nu\ \frac{d^\nu}{ds^\nu}\left(e^{s^2}f(s)\right)\bigg|_{s=0} \quad , \tag{25}$$

where

$$f(s) = \int_{-\infty}^{\infty} dv\ \frac{e^{-v^2/2}\cos\left(v\left(2s + z_0/b\right)\right)}{\left(1 + k_\nu^2a^2 + \frac{a^2}{b^2}v^2\right)^2} \quad . \tag{26}$$

This result can be further simplified by using the chain rule to replace $d^\nu/ds^\nu\ (e^{s^2}f(s))\big|_{s=0}$ by

$$\sum_p \frac{\nu!}{(\nu - 2p)!\,p!}\ \frac{d^{\nu-2p}}{ds^{\nu-2p}}\ f(s)\bigg|_{s=0} \quad .$$

We then obtain

$$\langle \nu, \mathbf{k}_\nu | H_1(\omega) | a \rangle = \frac{eE_0}{i\omega m} \left(\varepsilon \cdot \mathbf{P}_{c,v}(0)\right) \frac{C(0)}{\sqrt{2\pi}} N_\nu \sum_p \frac{\nu!}{(\nu - 2p)!\, p!} \frac{d^{\nu-2p}}{ds^{\nu-2p}} f(s)\Big|_{s=0} \quad . \tag{27}$$

Also, if we let $w \equiv (a/b)v$ and $\mu_\nu^2 \equiv 1 + k_\nu^2 a^2$, $f_s$ can be written

$$f(s) = -\frac{2b}{a} \frac{d}{d\mu_\nu^2} \int dw \, \frac{e^{-(b^2/2a^2)w^2} \cos(\Gamma w)}{\mu_\nu^2 + w^2} \quad , \tag{28}$$

where $\Gamma \equiv (2b/a)s + z_0/a$. This integral can be done [8] and the expression differentiated with respect to $\mu_\nu^2$ to obtain

$$\begin{aligned} f(s) = {} & \frac{\pi b}{4a\mu_\nu^3} e^{b^2\mu_\nu^2/2a^2} \left(1 - b^2\mu_\nu^2/a^2\right) \left[e^{\Gamma\mu_\nu} \mathrm{Erfc}\left(X_{\nu+}\right) + e^{-\Gamma\mu_\nu} \mathrm{Erfc}\left(X_{\nu-}\right)\right] \\ & - \frac{\pi b \Gamma}{4a\mu_\nu^2} e^{b^2\mu_\nu^2/2a^2} \left[e^{\Gamma\mu_\nu} \mathrm{Erfc}(X_{\nu+}) - e^{-\Gamma\mu_\nu} \mathrm{Erfc}(X_{\nu-})\right] \\ & + (\pi/2)^{1/2} \frac{b^2}{2a^2\mu_\nu^2} e^{b^2\mu_\nu^2/2a^2} \left[e^{\Gamma\mu_\nu} e^{-X_{\nu+}^2} + e^{-\Gamma\mu_\nu} e^{-X_{\nu-}^2}\right] , \end{aligned} \tag{29}$$

where $X_{\nu\pm} = \left[(b/a)\mu_\nu \pm z_0/b\right]/\sqrt{2}$ and Erfc is the complementary error function [8]. We can now use these results to obtain for W

$$W = \frac{64a^3 m_c e^2 |E_0|^2}{\pi^{1/2}\hbar^2 m^2 b\omega} \left|\hat{\varepsilon} \cdot \mathbf{P}_{c,v}(0)\right|^2 \sum_{\nu=0}^{\infty} \frac{\nu!}{2^\nu} \Theta\left(k_\nu^2\right) \left[\sum_p \frac{1}{(\nu - 2p)!\, p!} \frac{d^{\nu-2p}}{ds^{\nu-2p}} f(s)\Big|_{s=0}\right]^2 \tag{30}$$

This is our final result for W, which can be used in equation (14) to obtain the absorption coefficient $\alpha(\omega)$.

Before examining these results in any greater detail, we now consider the case of photoluminescence. For this, we assume that a steady-state non-equilibrium condition is maintained in the superlattice which produces a sharp quasi-Fermi level in the conduction band. Below this level, all conduction band states are occupied. Spontaneous emission of photons will result from transitions of these electrons into empty acceptor states. For photoluminescence, we need to determine the rate at which these photons are emitted. Detailed balance arguments given in appendix A lead to a relationship between microscopic induced and spontaneous transition probabilities, which can be expressed through the equation*

$$\left.\frac{dN_{q,\lambda}}{dt}\right|_{\text{spont.em}} = - \frac{\left.\frac{dN_{q,\lambda}}{dt}\right|_{\text{ind.abs.}}}{N_{q,\lambda}} \quad , \tag{31}$$

*In this equation, statistical factors are assumed equal to values which would maximize each ratio (see app A).

where $N_{\mathbf{q},\lambda}$ is the number of photons in mode $\mathbf{q},\lambda$ of the radiation field. To obtain the photoluminescence spectrum $R(\varepsilon)$, which was defined earlier, we need to multiply equation (31) by $\hbar\omega$, sum over all photon modes $\mathbf{q},\lambda$ consistent with their energy being in the interval $d\varepsilon$ at $\varepsilon$, and divide the result by the volume of the system. This gives

$$R(\varepsilon)d\varepsilon = \frac{\hbar\omega}{\Omega} \sum_{\mathbf{q},\lambda}' \left.\frac{dN_{\mathbf{q},\lambda}}{dt}\right|_{\text{spont.em.}} , \tag{32}$$

where the prime on the sum is a reminder of the energy restriction. But $N_{\mathbf{q},\lambda} = (u_{\mathbf{q},\lambda}\Omega/\hbar\omega)$, where $u_{\mathbf{q},\lambda}$ is the $\mathbf{q},\lambda$ contribution to the energy density in the field. If we use this together with equation (31), we obtain

$$R(\varepsilon)\, d\varepsilon = \frac{(\hbar\omega)^2}{\Omega} \sum_{\mathbf{q},\lambda}' \frac{\left.\frac{-dN_{\mathbf{q},\lambda}}{dt}\right|_{\text{ind.abs.}}}{\Omega u_{\mathbf{q},\lambda}} . \tag{33}$$

The quantity $-\hbar\omega dN_{\mathbf{q},\lambda}/dt|_{\text{ind.abs.}}$ is the rate at which energy is absorbed from the radiation field, which is precisely the quantity $I_0\alpha(\omega)\Omega$ calculated earlier (provided we take $\mathbf{q} = (0,0,q)$ and choose the same polarization $\hat{\varepsilon}$). Thus we can write

$$I_0\alpha_{\mathbf{q},\lambda}(\omega)\Omega = -\hbar\omega \left.\frac{dN_{\mathbf{q},\lambda}}{dt}\right|_{\text{ind.abs.}} . \tag{34}$$

Using this result in equation (33) along with the relation $u = nI_0/c$ gives

$$R(\varepsilon)\, d\varepsilon = \frac{\hbar\omega c}{n} \frac{1}{\Omega} \sum_{\mathbf{q},\lambda}' \alpha_{\mathbf{q},\lambda}(\omega) . \tag{35}$$

The only dependence of $\alpha_{\mathbf{q},\lambda}(\omega)$ on $\hat{q}$ and $\lambda$ comes from the square of the matrix element which contains the factor $|\hat{\varepsilon}_\lambda(\mathbf{q})\cdot\mathbf{P}_{c,v}(0)|^2$. Here $\hat{\varepsilon}_\lambda(\mathbf{q})$ ($\lambda = 1,2$) are the orthonormal polarization basis vectors which are orthogonal to $\hat{q}$ and defined according to some arbitrary (but definite) prescription. With this in mind we consider the sum

$$\frac{1}{\Omega} \sum_{\mathbf{q},\lambda}' |\hat{\varepsilon}_\lambda(\mathbf{q})\cdot\mathbf{P}_{c,v}(0)|^2 = \sum_\lambda \frac{q^2}{(2\pi)^3} \frac{dq}{d\varepsilon} d\varepsilon \int d\hat{q}\, |\hat{\varepsilon}_\lambda(\mathbf{q})\cdot\mathbf{P}_{c,v}(0)|^2 . \tag{36}$$

Using $\varepsilon = \hbar\omega = \hbar cq/n$, this becomes

$$\frac{1}{\Omega} \sum_{\mathbf{q},\lambda}' |\hat{\varepsilon}_\lambda(\mathbf{q})\cdot\mathbf{P}_{c,v}(0)|^2 = \frac{\omega^2 n^3}{2\pi^2\hbar c^3} \sum_\lambda \mathbf{P}_{c,v}(0)\cdot\overleftrightarrow{\pi}_\lambda\cdot\mathbf{P}^*_{c,v}(0) , \tag{37}$$

where we have defined $\overleftrightarrow{\pi}_\lambda = 1/4\pi \int d\hat{q}\, \hat{\varepsilon}_\lambda(\mathbf{q})\hat{\varepsilon}_\lambda(\mathbf{q})$.

One can replace $d\hat{q}$ by $d\hat{\varepsilon}$ and easily obtain $\overleftrightarrow{\pi}_\lambda = (1/3)\hat{q}_i\hat{q}_j\delta_{ij}$. If this is used in equation (37), one obtains

$$\frac{1}{\Omega}\sum_{\mathbf{q},\lambda}' |\hat{\varepsilon}_\lambda(\hat{q})\cdot\mathbf{P}_{c,v}(0)|^2 = \frac{\omega^2 n^3 d\varepsilon}{\pi^2\hbar^2c^3}\frac{1}{3}|\mathbf{P}_{c,v}(0)|^2 \quad . \tag{38}$$

Substituting this result into equation (35) then gives

$$R(\varepsilon) = \frac{n^2\omega^3}{\pi^2c^2}\langle\alpha_{\mathbf{q},\lambda}(\omega)\rangle \quad , \tag{39}$$

where $\langle\alpha_{\mathbf{q},\lambda}(\omega)\rangle$ $\left(=1/4\pi\int d\Omega_{\mathbf{q}}\,\alpha_{\mathbf{q},\lambda}(\omega)\right)$ is the angular average of $\alpha_{\mathbf{q},\lambda}(\omega)$, which is given by equation (14) for the case $\mathbf{q} = (0,0,q)$ and polarization $= \hat{\varepsilon}$. As shown above, $\langle\alpha(\omega)\rangle$ can be obtained simply from expressions for $\alpha(\omega)$ by replacing the quantity $|\hat{\varepsilon}\cdot\mathbf{P}_{c,v}(0)|^2$ which appears in the squared matrix element by the expression $1/3\ |\mathbf{P}_{c,v}(0)|^2$.

Equations (14), (30), and (39)* are the central results of this work. Under appropriate circumstances they can be used to gain insight into the photoluminescence and absorption spectra of doping superlattices.

## 4. PREDICTIONS AND DISCUSSION

Before the results obtained above are examined, a few comments will be made regarding their applicability.

The absorption spectrum given by equation (14) represents contributions to absorption from electronic transitions between localized acceptor states and extended (in two dimensions) conduction-band states. When $\hbar\omega$ is large enough to induce transitions between *extended* valence-band and extended conduction-band states, equation (14) will no longer apply, as these contributions were ignored in the analysis. It is also important to remember that this formula is applicable only when the exciting field is reasonably weak.† An intense external field will generate electron-hole pairs more rapidly than they can recombine, leading to a finite steady-state conduction-band charge density $n^{(2)}$ and an altered effective potential. In this instance, the potential used in obtaining the approximate eigenstates will be inappropriate, and equation (14) will provide only a qualitatively correct account of the spectrum.

---

*Care should be exercised in using equation (39) for the photoluminescence spectrum. In our calculation of $\alpha(\omega)$ we considered contributions from all acceptor levels. For photoluminescence, all acceptor states cannot be final states since some are already occupied. Instead, one should limit the range of integration in equation (14) to the distance required to contain a number of states equal to the total number of occupied states in the conduction band.

†In view of the nonlinear optical properties of this system, this constraint could be severe.

In the case of photoluminescence, similar considerations will apply. In particular, high pump laser intensities will produce steady states whose corresponding effective potentials are substantially different from the effective potential used in the calculation (which corresponded to $n^{(2)} = 0$). Despite these limitations of the theory, the more serious electronic structure calculations of Ruden and Döhler [4] support the qualitative picture presented in the model, at least for values of $n^{(2)}$ which are not excessive ($\gtrsim$50 percent of the available acceptor charge).

In what follows we examine the photoluminescence spectrum predicted by equation (39) for a superlattice characterized by a doping density of $1 \times 10^{18}$ $cm^{-3}$ and a period of 800 A. We will consider a range of charge densities $n^{(2)}$ since the spectra can be rather sensitive to this density. In order to apply equation (39), we need to determine two things. First, we need a reasonable representation of the manner in which the acceptor binding energies vary with distance from the center of the p regions. Variational calculations [5] support qualitatively the use of a binding energy profile similar to the one displayed schematically in figure 8. The binding energies are largest in the center of the p regions and decrease to small values near the edge of the p regions where the space charge field is largest (they can never go lower than the $\nu = 0$ oscillator level in the valence band since this marks the beginning of a continuum of states). To represent this state of affairs, the binding energies were modelled by the expression $\varepsilon_b(z) = \varepsilon_{bmax} e^{-\gamma z^2}$, where z measures distance from the center of the p regions and the parameters $\gamma$ and $\varepsilon_{bmax}$ are chosen judiciously. Finally, a choice must be made regarding the way in which *empty* acceptor states are distributed (among the occupied acceptor states) when charge is elevated into the conduction band in order to represent a specific steady-state configuration. We will assume that the empty acceptor states are those acceptors which occupy a region of finite thickness centered on the p regions (i.e., the highest energy states). The thickness of these regions is determined from the nonequilibrium charge density in the conduction band. For instance, if 50 percent of the available acceptor charge (electrons occupying acceptor states in the ground state) were elevated into the conduction band, then one half the thickness of the p layers would be neutral (200 A for a superlattice period of 800 A). We remind the reader that in such a case the binding energy profile would change since the "background" potential would be flattened in the central halves of the p regions.* The Gaussian profile function given above is flexible enough to account for this effect qualitatively since decreasing $\gamma$ (or $\varepsilon_{bmax}$) would flatten out the profile.

For the parameters we will consider, the quasi-Fermi energy $\varepsilon_F$ will always lie below the $\nu = 2$ oscillator level. In this case equation (30) simplifies considerably and can be combined with equations (14) and (39) to give, after some manipulation, the expression

$$R(\varepsilon) = D\xi^2 F(\xi) \quad , \tag{40}$$

*Another aspect of the binding energy profile which we have ignored in the present calculation is the inevitable dependence of the average acceptor wavefunction radius on its binding energy and hence position. Our present lack of information regarding the acceptor wavefunctions necessitates this.

where D is a constant,* $\xi$ is the photon energy in units of $\hbar\omega_0$, and $F(\xi)$ is given by the integral

$$F(\xi) = \int_{w_1}^{w_2} dw \left\{ I_0^2 \Theta\left(k_0^2\right)\left[1 - \Theta\left(k_{0f}^2\right)\right] + \frac{1}{2} I_1^2 \Theta\left(k_1^2\right)\left[1 - \Theta\left(k_{1f}^2\right)\right] \right\} , \qquad (41)$$

where $\Theta$ is the step function defined below equation (12),

$$k_n^2 = (2/b^2)\left\{\xi - (n + 1/2) + \varepsilon_a(\omega)/\hbar\omega_0\right\} ,$$

and

$$k_{nf}^2 \text{ is } k_n^2 \text{ with } \xi = \xi_f = \varepsilon_F/\hbar\omega_0 .$$

The functions $[1 - \Theta(k_n^2)]$ prevent photoluminescence contributions from states above the quasi-Fermi level while the functions $\Theta(k_n^2)$ prevent contributions from below the nth oscillator levels. The functions $I_0$ and $I_1$ are given by

$$\begin{aligned} I_0 = {} & \frac{\pi b}{2\mu_0 a} e^{b^2\mu_0^2/2a^2} e^{\Gamma\mu_0} \mathrm{Erfc}(X_{0+}) \left[\frac{1}{2\mu_0^2}\left(1 - b^2\mu_0^2/a^2\right) - \frac{b}{2a\mu_0} w\right] \\ & + \frac{\pi b}{2\mu_0 a} e^{b^2\mu_0^2/2a^2} e^{-\Gamma\mu_0} \mathrm{Erfc}(X_{0-}) \left[\frac{1}{2\mu_0^2}\left(1 - b^2\mu_0^2/a^2\right) - \frac{b}{2a\mu_0} w\right] \\ & + (\pi/2)^{1/2} \frac{b^2}{2a^2\mu_0^2} e^{b^2\mu_0^2/2a^2} \left[e^{\Gamma\mu_0} e^{-X_{0+}^2} + e^{-\Gamma\mu_0} e^{-X_{0-}^2}\right] . \end{aligned} \qquad (42)$$

$$\begin{aligned} I_1 = {} & -\frac{\pi b}{a\mu_1} e^{b^2\mu_1^2/2a^2} e^{\Gamma\mu_1} \mathrm{Erfc}(X_{1+}) \left[\frac{b^2}{2a^2}\left(\frac{b}{a}\mu_1 + w\right)\right] \\ & + \frac{\pi b}{a\mu_1} e^{b^2\mu_1^2/2a^2} e^{-\Gamma\mu_1} \mathrm{Erfc}(X_{1-}) \left[\frac{b^2}{2a^2}\left(\frac{b}{a}\mu_1 - w\right)\right] \\ & - (\pi/2)^{1/2} \frac{b}{a\mu_1^3} e^{b^2\mu_1^2/2a^2} \left(1 - b^2\mu_1^2/a^2\right)\left[e^{\Gamma\mu_1} e^{-X_{1+}^2} - e^{-\Gamma\mu_1} e^{-X_{1-}^2}\right] , \end{aligned} \qquad (43)$$

where $X_{\nu\pm} = \left[(b/a)\mu_\nu \pm w\right]/\sqrt{2}$ and $\Gamma = (b/a)w$. To define $\varepsilon_F$ we decide what fraction of the available acceptor charge is to be placed in the conduction band. The maximum available density $n_{max}^{(2)}$ (per unit area, per layer) is simply given by $N_d \ell/2$, while $\varepsilon_F$ is given by the solution to the equation

$$\left(m_c/\pi\hbar^2\right)\left(\varepsilon_F - \hbar\omega_0/2\right) = n^{(2)}$$

*D is given by $D = (1024\alpha/3\pi^{3/2}n)(N_d a^3)(e^2/\ell mc^2)(N_d/\ell m\hbar)\left|P_{c,v}(0)\right|^2$ where $\alpha$ (equal to $e^2/\hbar c$) is the fine structure constant.

when $\varepsilon_F$ lies between the $\nu = 0$ and $\nu = 1$ oscillator levels or

$$\left(m_c/\pi\hbar^2\right)\hbar\omega_0 + \left(2m_c/\pi\hbar^2\right)\left(\varepsilon_F - 3/2\hbar\omega_0\right) = n^{(2)}$$

when $\varepsilon_F$ lies between the $\nu = 1$ and $\nu = 2$ oscillator levels. In these expressions $m_c/\pi\hbar^2$ is the DOS (per unit area) in a two-dimensional system [3]. Finally, the limits of integration in equation (42) are given by

$$w_{1,2} = \left(2 \mp n^{(2)}/n^{(2)}_{max}\right)\frac{\ell}{4b} \quad . \tag{44}$$

In figure 9 a sequence of photoluminescence spectra is displayed for successively higher values of $n^{(2)}$. Each curve is labelled by the ratio $n^{(2)}/n^{(2)}_{max}$. Because of the theory's inability to accurately predict the

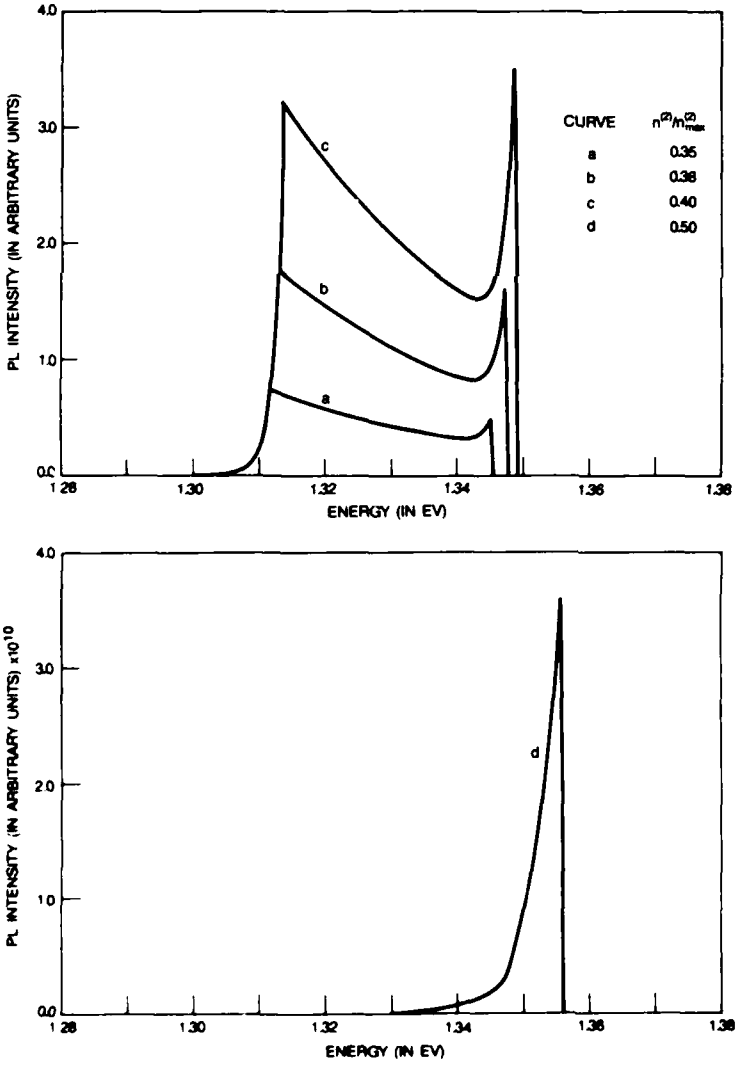


Figure 9. Theoretically predicted photoluminescence spectra for superlattice with parameters given in figure 1 (also $\varepsilon_{bmax}$ = 20 meV and $\lambda = 1/\gamma^2$ = 75 Å; see text).

effective gap, all effective gaps were set arbitrarily to 1.3 eV. Hence only differences in the horizontal axis are significant. The vertical scales are in arbitrary units. The curves were obtained by numerical evaluation* of $F(\xi)$ with the use of the parameters $\varepsilon_{bmax}$ = 20 meV and $\lambda$ ($\equiv 1/\gamma^2$) = 75 A. The nature of the curves is readily understood if attention is paid to two general considerations:

(a) The square of the matrix element of $H_1$ decreases exponentially with separation between the "centers" of the two wavefunctions involved. This implies that for a given acceptor position, higher oscillator levels will have significantly larger squared matrix elements since their wavefunctions extend further out from the oscillator center.

(b) For a given acceptor position and oscillator level, the squared matrix element of $H_1$ will decrease with increasing $\hbar\omega$ since this larger energy will go into conduction-band wavefunction phase oscillations, resulting in smaller overlap with the hydrogenic orbital.

Let us consider in detail the features of figure 9, curve a. The threshold for photoluminescence begins at 1.3 eV and rises exponentially to a maximum at 1.312 eV. This rise occurs because at threshold only states near the top of the acceptor profile (and hence further away from the oscillator well) are permitted to contribute. After $\hbar\omega$ has increased to above 1.312 eV, the entire range of acceptor energies is included, and a further increase in $\hbar\omega$ leads to a decay in the contributions due to consideration (b). This decay will continue until the threshold condition for the next ($\nu$ = 1) oscillator level is reached. One then gets an exponentially increasing contribution which will persist until either the quasi-Fermi energy is reached or $\hbar\omega$ has increased by 0.012 eV (1.312 eV - 1.300 eV), where another decay will begin. This is what happens as one goes from curve a to d. As the quasi-Fermi level increases, the second peak grows relative to the first until (in d) the second peak completely dwarfs the contributions from the $\nu$ = 0 level, leaving only an asymmetric peak. The behavior in figure 9 is generic and can be reproduced for a variety of parameter sets.

Figure 10 displays experimental photoluminescence results of Simpson et al [1] on a superlattice sample characterized by parameters similar to those considered theoretically. The photoluminescence intensity is in arbitrary units. When an attempt is made to compare the theoretical predictions with this spectrum, a serious difficulty arises. In the experiments, a pump laser is employed whose penetration depth into the superlattice is approximately 1000 to 2000 A. We are thus faced with the difficulty of choosing values of $n^{(2)}$ for each successive conduction-band well. Each well's effective gap (and relevant matrix elements) will then be changed by different amounts, and the total luminescence will be the sum of contributions from all layers. Such a calculation involves too many unknown parameters and would be unconvincing.

*The Fortran codes used are given in appendix B.

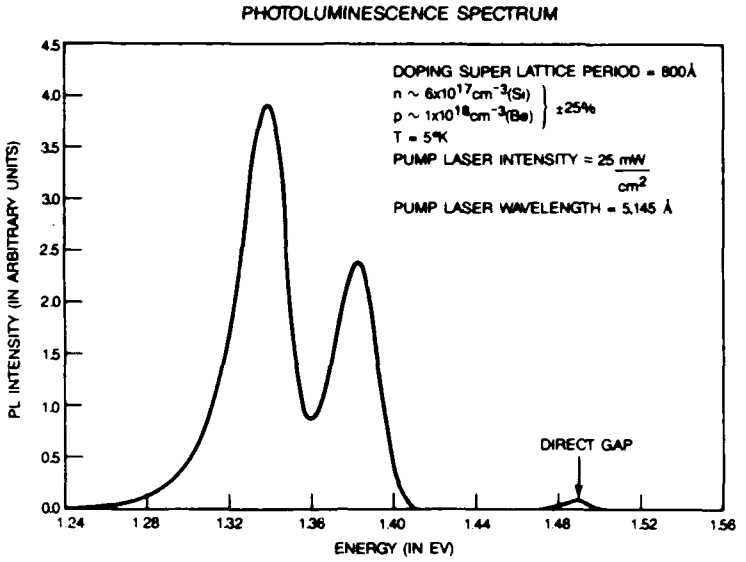


Figure 10. Experimental photoluminescence data of Simpson et al [1].

Because of this difficulty, we will postpone serious comparisons between theory and experiment until a less restrictive theory (or more compatible experiment) exists.

In concluding this report we list below a number of criticisms and comments relating to this model.

1. We have considered only the case where $N_d = N_a$, but this precise equality is experimentally unlikely. If $N_a$ were greater than $N_d$, the potential in the p regions would be flattened out in the ground state. On the other hand, if $N_d$ were greater than $N_a$, the n region potential would flatten and the ground state would be characterized by a nonzero conduction-band charge density $n^{(2)}$. The qualitative features of the theory would remain unchanged in these cases.

2. We have ignored details of the valence band in the analysis. It is hard to see how qualitative differences would arise because of this neglect. Although the effective mass theory would present more formidable mathematical problems in obtaining the acceptor state wavefunctions, the wavefunctions would still be qualitatively hydrogenic, with some distortion in shape--possibly flattened spheres with the thin dimension normal to the layers (these wavefunctions could also be obtained variationally if desired). The only aspect of this result which could be qualitatively important is that if the long dimension of the wavefunction became sizable, overlap with similar wavefunctions might produce extended (in two dimensions) acceptor states. This possibility remains to be adequately addressed.

3. We have ignored the effects of randomness in the analysis. It is clear that since the acceptors are at random positions throughout the

p-regions (with an average separation of 100 Å), an electron in the immediate neighborhood of a specific acceptor will feel a "background potential" (the potential due to all other changed acceptors and donors) which differs from one acceptor to another at a fixed z-coordinate. This variance in background potential was ignored in the analysis, and only the average background potential was included (which varied quadratically with distance from the center of the p-region). It is difficult to estimate the size of this variance since charge carrier screening of the potential is probably substantial. (A simple model including screening is currently being studied to give some idea of this variance in background potential. The results of this investigation will be presented in a future publication.) In any event, this phenomenon will lead to a distribution of binding energies at each coordinate $z_0$. One would then have to integrate over this impurity band for each $z_0$, leading to obvious changes in the photoluminescence spectrum.

4. In the analysis we ignored the fact that decreasing binding energy will mean increasing acceptor state extension. A more accurate treatment would have allowed the acceptor Bohr radius a to be a function of z.

5. Homogeneous line broadening was ignored in the analysis but would result in a smoothing out of sharp spectral features in figure 9.

6. The reader is reminded that the spectra displayed in figure 9 are very sensitive to the distribution of occupied acceptor states. In particular, the $10^{10}$ factor in figure 9(d) comes primarily from the fact that higher densities provide empty acceptor states closer to the conduction-band wells. A different acceptor state distribution would result in an entirely different spectrum.

## ACKNOWLEDGEMENTS

I take this opportunity to thank T. B. Simpson, T. Bahder, R. P. Leavitt, C. A. Morrison, and P. P. Ruden for fruitful discussions and G. Turner for computer assistance. Additional thanks go to T. B. Simpson for providing motivation.

## REFERENCES


(1) T. B. Simpson, J. E. Anthony, T. R. AuCoin, J. Bruno, J. J. Winter, and R. P. Leavitt, Bull. Am. Phys. Soc. 31 (3) (1986), 558.

(2) J. M. Luttinger and W. Kohn, Phys. Rev. 97 (1955), 879.

(3) N. W. Ashcroft and N. David Mermin, Solid State Physics, Holt Reinhart and Winston (1976).

(4) P. Ruden and G. H. Döhler, Phys. Rev. B27 (1983), 3538.

(5) R. P. Leavitt and T. B. Simpson, Bull. Am. Phys. Soc. 31 (3) (1986), 558.

(6) B. R. Nag, Electron Transport in Compound Semiconductors, Springer Verlag (1980).

(7) E. Merzbacher, Quantum Mechanics, John Wiley and Sons Inc (1970).

(8) Tables of Integral Transforms, A. Erdélyi, editor, Bateman Manuscript Project, Vol 1: 1.4(15), McGraw Hill (1954).

# APPENDIX A.--RELATIONSHIP BETWEEN INDUCED AND SPONTANEOUS TRANSITION PROBABILITY

The principle of detailed balance permits one to establish a relationship between the microscopic transition probabilities for induced emission and spontaneous emission in a physical system without resorting to the otherwise unnecessary procedure of quantizing the electromagnetic field.

Consider a superlattice in thermal equilibrium with the radiation field, and focus attention on two specific states in the superlattice, say "1" and "2" with energies $\varepsilon_1$ and $\varepsilon_2$ ($<\varepsilon_1$), respectively. We assume that electrons making transitions between these states will be accompanied by emission and absorption of photons of type $\mathbf{q},\lambda$ changing the state of the radiation field. If we let $N_{\mathbf{q},\lambda}$ represent the number of photons in this mode of the field, we can write for the total rate at which $N_{\mathbf{q},\lambda}$ changes because of occupancy changes in states 1 and 2:

$$\frac{dN_{\mathbf{q},\lambda}}{dt} = \left.\frac{dN_{\mathbf{q},\lambda}}{dt}\right|_{\text{ind.em.}} + \left.\frac{dN_{\mathbf{q},\lambda}}{dt}\right|_{\text{spont.em.}} + \left.\frac{dN_{\mathbf{q},\lambda}}{dt}\right|_{\text{ind.abs.}} .$$

The induced absorption and emission rates are proportional to the number of photons present and to the probability that the appropriate initial states are occupied and final states unoccupied:

$$\left.\frac{dN_{\mathbf{q},\lambda}}{dt}\right|_{\text{ind.em.}} = BN_{\mathbf{q},\lambda}P_2(1 - P_1) ,$$

$$\left.\frac{dN_{\mathbf{q},\lambda}}{dt}\right|_{\text{ind.abs.}} = -BN_{\mathbf{q},\lambda}P_1(1 - P_2) .$$

The fact that both have the same coefficient B follows from microscopic reversibility. On the other hand, the spontaneous emission rate simply depends on the probability that state 2 is occupied and state 1 unoccupied:

$$\left.\frac{dN_{\mathbf{q},\lambda}}{dt}\right|_{\text{spont.em.}} = AP_2(1 - P_1) .$$

When thermal equilibrium prevails, $dN_{\mathbf{q},\lambda}/dt = 0$ or

$$AP_2(1 - P_1) + BN_{\mathbf{q},\lambda}P_2(1 - P_1) = BN_{\mathbf{q},\lambda}P_1(1 - P_2) ,$$

which gives

$$A = BN_{\mathbf{q},\lambda}\left[\frac{P_1 - P_2}{P_2(1 - P_1)}\right] .$$

But in equilibrium $P(E) = \left[1 + e^{(E-\mu)/kT}\right]^{-1}$ and a little algebra reduces the bracketed term to $e^{\hbar\omega/kT} - 1$, which is precisely the inverse of the Planck

distribution $N_{\mathbf{q},\lambda} = (e^{\hbar\omega/kT} - 1)^{-1}$. Thus A = B, and for a system in which we know from first principles the rate $dN_{\mathbf{q},\lambda}/dt\big|_{\text{ind.abs.}}$, we can write

$$\left.\frac{dN_{\mathbf{q},\lambda}}{dt}\right|_{\text{spont.em.}} = B = \frac{\left. - \frac{dN_{\mathbf{q},\lambda}}{dt}\right|_{\text{ind.abs.}}}{N_{\mathbf{q},\lambda}} ,$$

where the statistical factors are assumed equal to $P_1 = 1$, $P_2 = 0$ for induced absorption and $P_1 = 0$, $P_2 = 1$ for spontaneous emission.

# APPENDIX B.--FORTRAN CODES FOR PHOTOLUMINESCENCE CALCULATION

Appendix B lists the Fortran code used in the numerical evaluation of the integral given by equation (41) in the main body of this report.

```
C***************** PHOTOLUMINESCENCE CALCULATION *****************
C$ SCREEN
C$ WRITE SYS$OUTPUT "COMPILING"
C$ FORT PLSPEC
C$ WRITE SYS$OUTPUT "LINKING"
C$ LINK PLSPEC,XYPLOT,HDL$LIB/L,CMLIB/L,DISSPLA/L,GH/L
C
C          ****** BEGIN MAIN PROGRAM ******
C
        IMPLICIT REAL*8 (A-H,O-Z)
        REAL*4 SENERGY(1000),SPLSPEC(1000),YB(1000)
        CHARACTER*1 NANS
        DIMENSION ENERGY(1000),PLSPEC(1000),IWORK(100),WORK(400)
        COMMON/CONSTANTS/X,A,B,PI,SPI2,STWO,SEP,EGPEXP,EBMAX,SP,ALPHA
        COMMON/EXTRA/UPLIM,GAMMA
        EXTERNAL F,DERFC,EA
C
C                DEFINE FUNCTIONS
C
        YY(X,W)=2.*(A/B)**2*(X-0.5+(EA(W)/SEP))
        AMU(X,W)=DSQRT(1.+YY(X,W))
        EB(Z)=EBMAX*DEXP(-ALPHA*Z**2)
C
C                ENTER DOPING PARAMETERS
C
        TYPE *,'ENTER DOPING DENSITY IN UNITS OF 1.0X10(18) CM-3'
        ACCEPT *,DD
        DD=1.0D18*DD
        TYPE *,'ENTER SUPERLATTICE PERIOD IN UNITS OF ANGSTROMS'
        ACCEPT *,SP
        SP=1.0D-8*SP
C
C                DEFINE VARIOUS CONSTANTS
C
        EG=1.424
        AK=12.5
        AM0=9.1095D-28
        AMV=0.50D0*AM0
        AMC=0.067D0*AM0
        HBAR=1.05459D-27
        EC=4.80324D-10
        CONV=1.60219D-12
        A=((HBAR/EC)**2)*AK/AMV
        BBEEV=(AMV/(AM0*AK**2))*13.60568D0
        BBMEV=1000.D0*BBEEV
        BBE=CONV*BBEEV
        PI=4.D0*DATAN(1.D0)
        SPI2=DSQRT(PI/2.D0)
        STWO=SQRT(2.D0)
C
C                CALCULATE OMEGA0, OSCILLATOR ENERGY HBAR*OMEGA0,
C                AND ZERO POINT AMPLITUDE B
C
        OMEGA0=EC*DSQRT(4.D0*PI*DD)/DSQRT(AMC*AK)
        SEP=HBAR*OMEGA0
        SEPEV=SEP/CONV
        SEPMEV=1000.D0*SEPEV
        TYPE 1,SEPMEV
1       FORMAT(/,20X,'HBAR*OMEGA0=',F7.3,'mev',/)
        B=SQRT(HBAR/(AMC*OMEGA0))
        BANG=1.0D8*B
```

APPENDIX B

```
C
C                CALCULATE U0 AND EEG(EFF ENERGY GAP)
C
        U0=(AMC*(OMEGA0*SP)**2)/(32.D0*CONV)
        EEG=EG-2.D0*U0
        IF(EEG.GE.0.D0)GO TO 2
        TYPE *,'STOP IN PLSPEC: EFF ENERGY GAP IS NEGATIVE'
        STOP
2       CONTINUE
C
C                DETERMINE 2-D DENSITY OF STATES
C                (NOTE THAT BECAUSE OF UNITS, HBAR**2 IS TOO SMALL
C                AND SO HAS BEEN REPLACED WITH HBAR. CORRECTIONS ARE
C                MADE IN APPROPRIATE PLACES)
C
        RHO2D=AMC/(PI*HBAR)
        STATES=RHO2D*SEP/HBAR
C
C                DETERMINE NON-EQUILIBRIUM CHARGE DENSITY
C
        AVAILC=DD*SP/2.D0
        TYPE 4,AVAILC
4       FORMAT(/,' MAX. NON-EQUILIBRIUM CHARGE DENSITY=',D8.3,'cm-2',/)
        TYPE *,'ENTER ACTUAL NON-EQUILIBRIUM CHARGE DENSITY AS A FRACTIO
     CN OF THE ABOVE STATED MAXIMUM (NUMBER BETWEEN 0. AND 1.)'
        ACCEPT *,FRAC
        CHDENS=FRAC*AVAILC
C
C                CONSTRUCT MODEL BINDING ENERGY PROFILE
C
        TYPE 23,BBMEV
23      FORMAT(' ACCEPTOR BINDING ENERGY IN UNDOPED CRYSTAL IS',F7.3,'me
     Cv',/,' ENTER MAX BINDING ENERGY IN SUPERLATTICE IN mev',/)
        ACCEPT *,EBMAX
        EBMAX=EBMAX*CONV/1000.D0
        TYPE 24,BANG
24      FORMAT(' OSCILLATOR ZERO POINT AMPLITUDE IS',F7.2,'angstroms',/,
     C' ENTER LENGTH SCALE FOR BINDING ENERGY DECREASE IN angstroms',/)
        ACCEPT *,ALPHA
        ALPHA=ALPHA/BANG
        ALPHA=1.D0/(ALPHA**2)

C
C                DETERMINE INTEGRATION LIMITS AND MAX. ACCEPTOR ENERGY
C                RANGE TO BE ENCOUNTERED
C
        ACCTHK=FRAC*SP/2.D0
        WMIN=0.5D0*(SP-ACCTHK)/B
        WMAX=0.5D0*(SP+ACCTHK)/B
        TYPE *,'WMIN=',WMIN,'      WMAX=',WMAX
        WZ=WMAX-0.5D0*SP/B
        ERANGE=EBMAX-EB(WZ)
        ERANGEMEV=1000.D0*ERANGE/CONV
        TYPE 333,ERANGEMEV
333     FORMAT(' ENERGY RANGE=',F6.2,'MEV')
C
C                DETERMINE FERMI LEVEL
C
        CHMAX=3.D0*STATES
        IF(CHDENS.GE.CHMAX)THEN
        TYPE *,'STOP IN PLSPEC: PROGRAM WONT PRESENTLY HANDLE SITUATIONS
     CINVOLVING OSCILLATOR LEVELS 3 OR HIGHER'
        STOP
        END IF
```

```
      IF(CHDENS.LT.STATES)THEN
      EFERMI=HBAR*CHDENS/RHO2D+SEP/2.D0
      ELSE
      X1=0.5D0*((CHDENS/STATES)-1)
      EFERMI=(1.D0+X1)*SEP+SEP/2.D0
      END IF
      EFEV=EFERMI/CONV
      EFMEV=EFEV*1000.D0
      TYPE 8,EFMEV
8     FORMAT(/,' FERMI ENERGY=',F7.3,'mev',/)
C
C             DETERMINE RANGE OF ENERGIES FOR PL SPECTRUM
C
      TYPE 11,EEG
11    FORMAT(' EFFECTIVE ENERGY GAP (THEO)=',F5.3,'ev',/)
      TYPE *,'ENTER EXPERIMENTAL EFFECTIVE GAP IN ev'
      ACCEPT *,EGPEXP
      EGPEXP=EGPEXP*CONV
      EMIN=EGPEXP/SEP-1.D0/10.D0
      EMAX=(EGPEXP+EBMAX)/SEP+EFERMI/SEP-1.D0/2.D0+1.D0/10.D0
      RANGE=EMAX-EMIN
      UPLIM=(EGPEXP+EFERMI-SEP/2.D0)/SEP
C
C             SET ENERGY STEPS IN PL SPEC
C
      STEPS=200.D0
      ISTEPS=STEPS
      DELTAE=RANGE/STEPS
C
C             DEFINE PARAMETERS FOR INTEGRATION ROUTINE
C
      EPSABS=0.D0
      EPSREL=1.0D-2
      LIMIT=100
      LENW=400
C
C             BEGIN LOOP TO PRODUCE PLSPEC
C
      NUM=ISTEPS+1
      DO 22 I=1,NUM
      AI=I-1
      ENERGY(I)=EMIN+AI*DELTAE
      X=ENERGY(I)
      CALL DQAGS(F,WMIN,WMAX,EPSABS,EPSREL,RESULT,ABSERR,NEVAL,IER,
     C LIMIT,LENW,LAST,IWORK,WORK)
      TYPE *,'IER=',IER,'     ITER=',I
      PLSPEC(I)=RESULT*X**2
22    CONTINUE
C
C             DEFINE SINGLE PRECISION VARIABLES FOR PLOT ROUTINE
C
      DO 75 I=1,NUM
      SPLSPEC(I)=PLSPEC(I)
      SENERGY(I)=SEP*ENERGY(I)/CONV
      WRITE(32,*)SENERGY(I),SPLSPEC(I)
75    CONTINUE
C
C             BROADEN PL SPECTRUM ??
C
      TYPE *,' DO YOU WISH TO BROADEN LEVELS ? (Y/N)'
      ACCEPT 44,NANS
44    FORMAT(A1)
```

```
      IF(NANS.EQ.'Y')THEN
      TYPE *,' ENTER BROADENING WIDTH IN mEV '
      ACCEPT *,GAMMA
      GAMMA=GAMMA/1000.D0
      CALL BROADEN(SENERGY,SPLSPEC,YB,NUM)
      CALL XYPLOT(SENERGY,YB,NUM)
      ELSE
C
C               PLOT WITHOUT BROADENING
C
      CALL XYPLOT(SENERGY,SPLSPEC,NUM)
      END IF
      TYPE *,' DO YOU WISH TO BROADEN THE  SPECTRUM ? (Y/N)'
      ACCEPT 44,NANS
      IF(NANS.EQ.'Y')THEN
      TYPE *,' ENTER BROADENING WIDTH IN mEV '
      ACCEPT *,GAMMA
      GAMMA=GAMMA/1000.D0
      CALL BROADEN(SENERGY,SPLSPEC,YB,NUM)
      CALL XYPLOT(SENERGY,YB,NUM)
      ELSE
      END IF
C
C               END OF MAIN PROGRAM
C
      TYPE *,'FORTRAN STOP'
      END

C
C     ******  BEGIN SUBROUTINES  ******
C
      REAL*8  FUNCTION F(W)
      IMPLICIT REAL*8 (A-H,O-Z)
      COMMON/CONSTANTS/X,A,B,PI,SPI2,STWO,SEP,EGPEXP
      COMMON/EXTRA/UPLIM,GAMMA
C
C               DEFINE FUNCTIONS
C
      YY(X,W)=2.D0*(X-0.5D0+EA(W)/SEP)*(A/B)**2
      AMU(X,W)=DSQRT(1.D0+YY(X,W))
C
C               DETERMINE IF Y(X) > 0 :IF YES, EVALUATE FIRST TERM OF
C               INTEGRAND. IF NO,SET INTEGRAND TO ZERO AND RETURN
C

      F=0.D0
      Y=YY(X,W)
      YO=YY(UPLIM,W)
      IF((Y.LE.0.D0).OR.(Y.GE.YO))THEN
      F=0.D0
      RETURN
      ELSE
      T1=AMU(X,W)
      T2=DEXP(((B*T1)/(STWO*A))**2)
      GAM=W*B/A
      T3=DEXP(GAM*T1)
      XOP=B*T1/(STWO*A)+W/STWO
      XOM=XOP-STWO*W
      Z1=PI*B*T2*T3*DERFC(XOP)*((1.D0-(B*T1/A)**2)/2.D0/T1**2-GAM/2.D0/T1)
      Z1=Z1/(2.D0*T1*A)
      Z2=PI*B*T2*DERFC(XOM)*((1.D0-(B*T1/A)**2)/2.D0/T1**2+GAM/2.D0/T1)
      Z2=Z2/(2.D0*T1*T3*A)
      Z3=SPI2*(B**2)*T2*(T3*DEXP(-XOP**2)+DEXP(-XOM**2)/T3)/2.D0/(T1*A)**2
      T4=Z1+Z2+Z3
      F=T4**2
      END IF
```

```
C
C               DETERMINE IF Y(X-1) > 0 : IF YES EVALUATE SECOND TERM OF
C               INTEGRAND. IF NO, RETURN
C
      Y=YY(X-1.D0,W)
      Y1=YY(UPLIM-1.D0,W)
      IF((Y.LE.0.D0).OR.(Y.GE.Y1))THEN
      RETURN
      ELSE
      T1=AMU(X-1.D0,W)
      T2=DEXP(((B*T1)/(STWO*A))**2)
      T3=DEXP(GAM*T1)
      XOP=B*T1/(STWO*A)+W/STWO
      XOM=XOP-STWO*W
      Z1=PI*B*T2*T3*DERFC(XOP)/(A*T1)
      Z1=Z1*(B**2*(B*T1/A+W)/(2.D0*A**2))
      Z2=(PI*B*T2/T3)*DERFC(XOM)/(A*T1)
      Z2=Z2*(B**2*(B*T1/A-W)/(2.D0*A**2))
      Z3=SPI2*B*T2*(1.D0-(B*T1/A)**2)/(A*T1**3)
      Z3=Z3*(T3*DEXP(-XOP**2)-DEXP(-XOM**2)/T3)
      T5=-Z1+Z2-Z3
      F=F+0.5D0*T5**2
      END IF
      RETURN
      END

      REAL*8 FUNCTION EA(W)
      IMPLICIT REAL*8 (A-H,O-Z)
      COMMON/CONSTANTS/X,A,B,PI,SPI2,STWO,SEP,EGPEXP,EBMAX,SP,ALPHA
      EB(Z)=EBMAX*DEXP(-ALPHA*Z**2)
      WW=W-SP/(2.D0*B)
      EA=EB(WW)-EBMAX-EGPEXP+SEP/2.D0
      RETURN
      END

      SUBROUTINE BROADEN(X,Y,YB,NUM)
      IMPLICIT REAL*8 (A-H,O-Z)
      REAL*4 X(1000),Y(1000),YB(1000)
      COMMON/CONSTANTS/DX,A,B,PI,SPI2,STWO,SEP,EGPEXP,EBMAX,SP,ALPHA
      COMMON/EXTRA/UPLIM,GAMMA
      LORENTZ(A,B)=(GAMMA/PI)/((A-B)**2+GAMMA**2)
      RANGE=X(NUM)-X(1)
      WEIGHT=X(2)-X(1)
      IDEL=IIDINT(RANGE/GAMMA)
      ANUM=NUM
      AIDEL=IDEL
      L=IIDINT(ANUM/AIDEL)
      DO 12 I=1,NUM
      YB(I)=0.D0
      XC=X(I)
      J=I+L
      DO 12 M=J-L,J+L
      IF(((M-L).LE.0).OR.((M-L).GT.NUM))THEN
      YB(I)=YB(I)+0.D0
      ELSE
      YY=Y(M-L)
      XX=X(M-L)
      YB(I)=YB(I)+YY*WEIGHT*LORENTZ(XX,XC)
      END IF
      CONTINUE
      RETURN
      END
```

DISTRIBUTION

ADMINISTRATOR
DEFENSE TECHNICAL INFORMATION CENTER
ATTN DTIC-DDA (12 COPIES)
CAMERON STATION, BUILDING 5
ALEXANDRIA, VA 22304-6145

ENGINEERING SOCIETIES LIBRARY
ATTN ACQUISITIONS DEPT
345 EAST 47TH STREET
NEW YORK, NY 10017

COMMANDER
US ARMY MATERIALS & MECHANICS
RESEARCH CENTER
ATTN DRXMR-TL, TECH LIBRARY BR
WATERTOWN, MA 02172

COMMANDER
US ARMY RESEARCH OFFICE (DURHAM)
PO BOX 12211
ATTN B. D. GUENTHER
ATTN R. J. LONTZ
ATTN C. BOGOSIAN
ATTN M. STROSCIO
RESEARCH TRIANGLE PARK, NC 27709

COMMANDER
US ARMY ELECTRONICS TECHNOLOGY
& DEVICES LABORATORY
ATTN G. IAFRATE
ATTN R. LAREAU
ATTN D. SMITH
ATTN L. YERKE
ATTN T. AUCOIN
FT MONMOUTH, NJ 07703

DIRECTOR
NAVAL RESEARCH LABORATORY
ATTN CODE 2620, TECH LIBRARY BR
ATTN A. M. KRIMAN
WASHINGTON, DC 20375

ATT BELL LABORATORIES
ATTN B. A. WILSON
ATTN A. Y. CHO
600 MOUNTAIN AVE
MURRAY HILL, NJ 07974

BERKELEY RESEARCH ASSOCIATES, INC
PO BOX 852
ATTN R. D. TAYLOR
SPRINGFIELD, VA 22150

DIRECTOR
ADVISORY GROUP ON ELECTRON DEVICES
ATTN SECTRY, WORKING GROUP D
201 VARICK STREET
NEW YORK, NY 10013

GOVERNMENT SYS. DIV
RCA MS 108-102
ATTN S. KATZ
MOORESTOWN, NJ 08057

HONEYWELL PHYSICAL SCIENCES CTR
ATTN P. P. RUDIN
10701 LYNDALE AVENUE SOUTH
BLOOMINGTON, MN 55420

MARTIN MARIETTA
ATTN F. CROWNE
ATTN R. LEAVITT
ATTN J. LITTLE
ATTN T. WORCHESKY
1450 SOUTH ROLLING ROAD
BALTIMORE, MD 21226

SCIENTIFIC APPLICATIONS, INC.
ATTN B. GORDON
3 DOWNING RD
HANOVER, NH 03755

UNIVERSITY OF HAWAII
DEPT OF PHYSICS
ATTN C. VAUSE
2505 CORREA RD
HONOLULU, HI 96822

UNIVERSITY OF MARYLAND
DEPT OF ELEC. ENG.
ATTN C. H. LEE
COLLEGE PARK, MD 20742

PENN STATE UNIVERSITY
DEPT OF PHYSICS
ATTN M. R. GIRI
HAZLETON, PA 18201

US ARMY LABORATORY COMMAND
ATTN COMMANDER, AMSLC-CG
ATTN TECHNICAL DIRECTOR, AMSLC-TD

INSTALLATION SUPPORT ACTIVITY
ATTN RECORD COPY, SLCIS-IM-TS
ATTN LIBRARY, SLCIS-IM-TL (3 COPIES)
ATTN LIBRARY, SLCIS-IM-TL (WOODBRIDGE)
ATTN TECHNICAL REPORTS BRANCH,
SLCIS-IM-TR
ATTN LEGAL OFFICE, SLCIS-CC

DISTRIBUTION (cont'd)

HARRY DIAMOND LABORATORIES
ATTN D/DIVISION DIRECTORS
ATTN CHIEF, SLCHD-NW-E
ATTN CHIEF, SLCHD-NW-EC
ATTN CHIEF, SLCHD-NW-ED
ATTN CHIEF, SLCHD-NW-EE
ATTN CHIEF, SLCHD-NW R
ATTN CHIEF, SLCHD-NW-RA
ATTN CHIEF, SLCHD-NW-RC
ATTN CHIEF, SLCHD-NW-RE
ATTN CHIEF, SLCHD-NW-RH
ATTN CHIEF, SLCHD-NW-RI
ATTN CHIEF, SLCHD-NW-P
ATTN CHIEF, SLCHD-RT-RA
ATTN CHIEF, SLCHD-RT-RB
ATTN C. S. KENYON, SLCHD-NW-EC
ATTN A. HARMANN, SLCHD-NW-EC
ATTN D. TROXEL, SLCHD-NW-EC
ATTN T. BAHDER, SLCHD-RT-RA
ATTN P. BRODY, SLCHD-RT-RA
ATTN H. DROPKIN, SLCHD-RT-RA
ATTN E. EDWARDS, SLCHD-RT-RA
ATTN K. HALL, SLCHD-RT-RA
ATTN M. HANSEN, SLCHD-RT-RA
ATTN G. HAY, SLCHD-RT-RA
ATTN E. KATZEN, SLCHD-RT-RA
ATTN C. MORRISON, SLCHD-RT-RA
ATTN R. NEIFELD, SLCHD-RT-RA
ATTN C. PENNISE, SLCHD-RT-RA
ATTN A. SEMENDY, SLCHD-RT-RA
ATTN G. SIMONIS, SLCHD-RT-RA
ATTN T. SIMPSON, SLCHD-RT-RA
ATTN M. STEAD, SLCHD-RT-RA
ATTN J. STELLATO, SLCHD-RT-RA
ATTN M. TOBIN, SLCHD-RT-RA
ATTN G. TURNER, SLCHD-RT-RA
ATTN R. FELOCK, SLCHD-RT-RB
ATTN C. GARVIN, SLCHD-RT-RB
ATTN J. GOFF, SLCHD-RT-RB
ATTN N. KARAYIANIS, SLCHD-RT-RB
ATTN D. McGUIRE, SLCHD-RT-RB
ATTN P. PELLEGRINO, SLCHD-RT-RB
ATTN F. B. MCLEAN, SLCHD-NW-RC
ATTN J. BRUNO, SLCHD-RT-RA (20 COPIES)

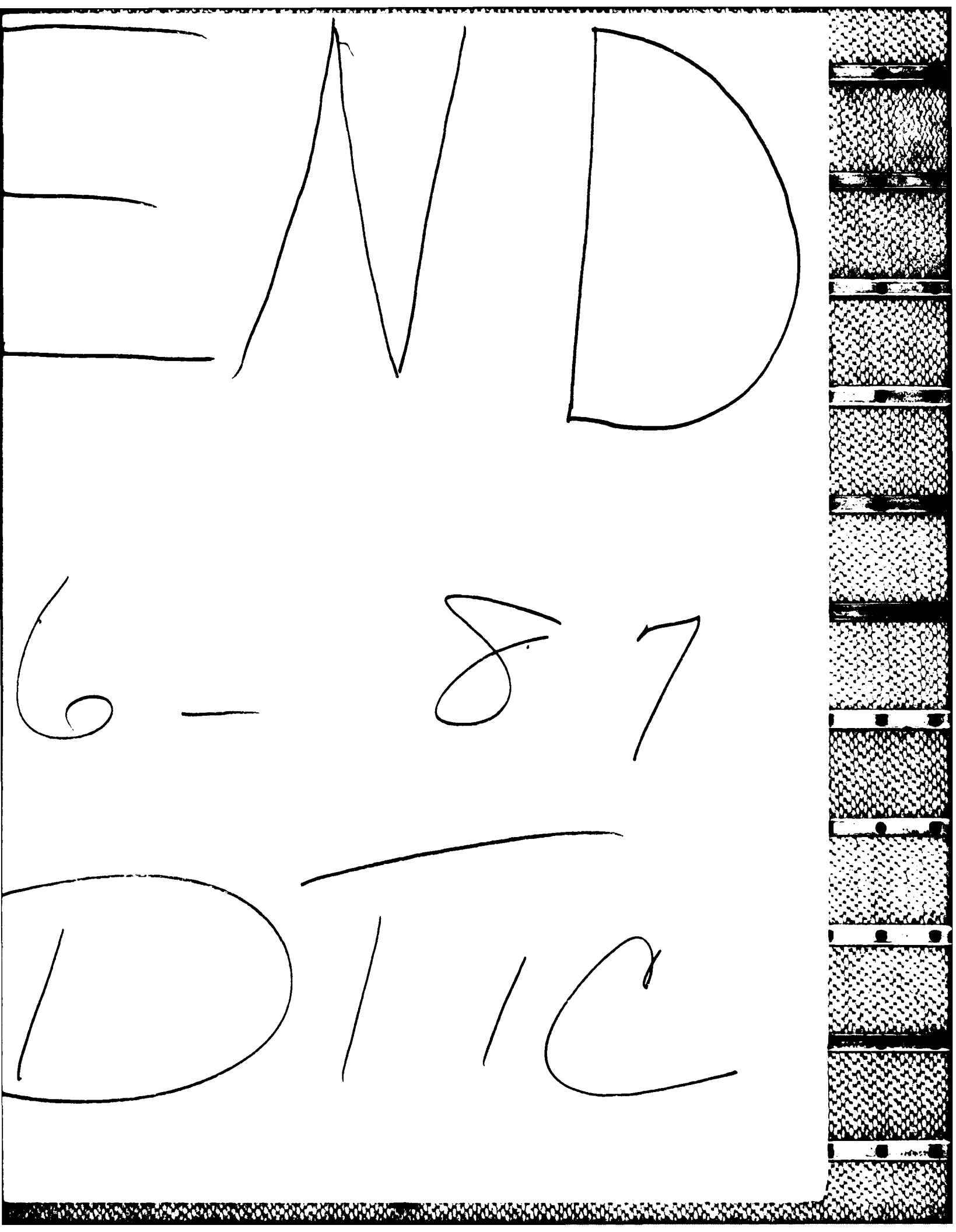
END
6-87
DTIC